iScience

CellPress
OPEN ACCESS

Article

miR-1307 promotes hepatocarcinogenesis by CALR-OSTC-endoplasmic reticulum protein folding pathway

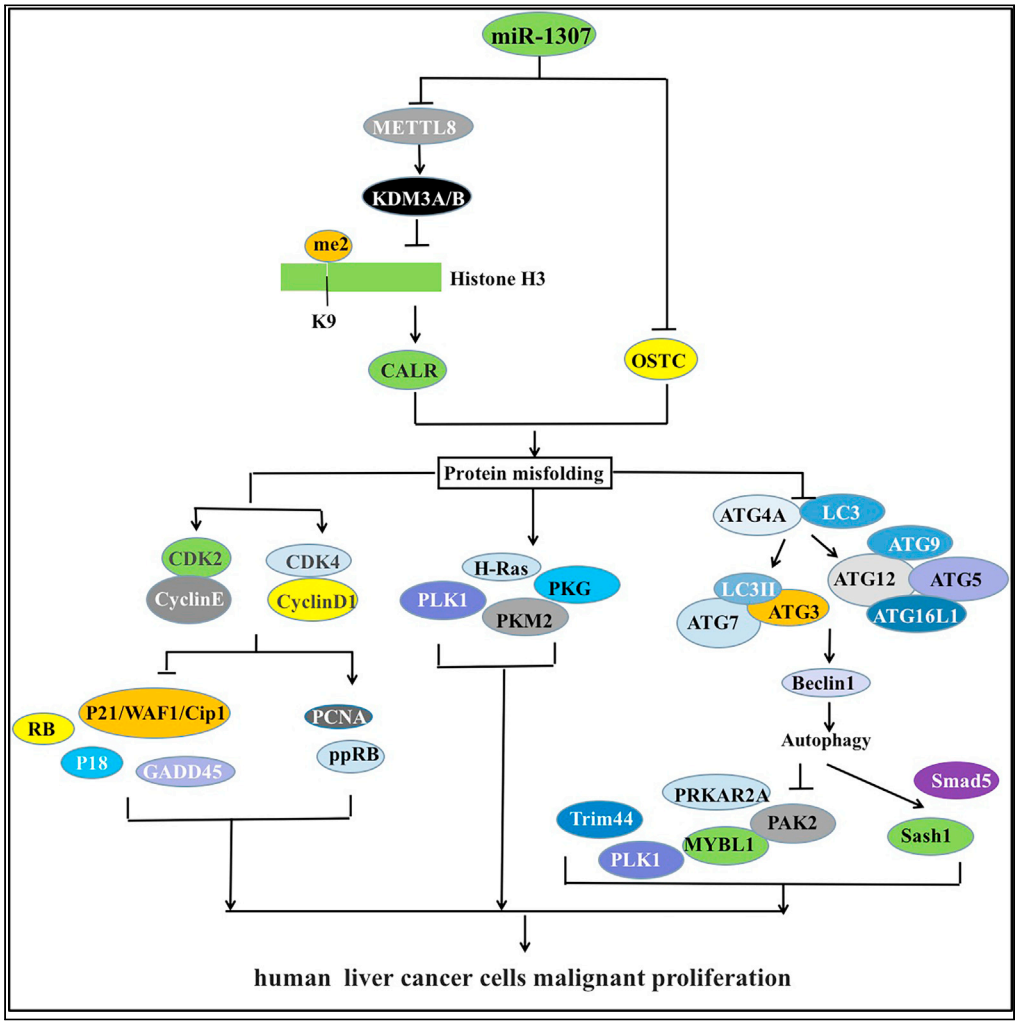

Sijie Xie, Xiaoxue Jiang, Rushi Qin, ..., Liyan Wang, Yingjie Chen, Dongdong Lu

ludongdong@tongji.edu.cn

Highlights

miR-1307 inhibits methyltransferase protein 8

miR-1307 enhances the expression of CALR

miR-1307 promotes hepatocarcinogenesis by CALR-OSTC pathway

Xie et al., iScience 24, 103271
November 19, 2021 © 2021 The Authors.
https://doi.org/10.1016/j.isci.2021.103271

iScience

CellPress
OPEN ACCESS

Article

miR-1307 promotes hepatocarcinogenesis by CALR-OSTC-endoplasmic reticulum protein folding pathway

Sijie Xie,[1,2] Xiaoxue Jiang,[1,2] Rushi Qin,[1,2] Shuting Song,[1] Yanan Lu,[1] Liyan Wang,[1] Yingjie Chen,[1] and Dongdong Lu[1,3,*]

SUMMARY

miR-1307 is highly expressed in liver cancer and inhibits methyltransferase protein8. Thereby, miR-1307 inhibits the expression of KDM3A and KDM3B and increases the methylation modification of histone H3 lysine 9, which enhances the expression of endoplasmic-reticulum-related gene CALR. Of note, miR-1307 weakens the binding ability of OSTC to CDK2, CDK4, CyclinD1, and cyclinE and enhances the binding ability of CALR to CDK2, CDK4, CyclinD1, and cyclinE, decreasing of p21WAF1/CIP1, GADD45, pRB, and p18, and decreasing of ppRB. Furthermore, miR-1307 increases the activity of H-Ras, PKM2, and PLK1. Strikingly, miR-1307 reduces the binding ability of OSTC to ATG4 and enhances the binding ability of CALR to ATG4. Therefore, miR-1307 reduces the occurrence of autophagy based on ATG4-LC3-ATG3-ATG7-ATG5-ATG16L1-ATG12-ATG9-Beclin1. In particular, miR-1307 enhances the expression of PAK2, PLK1, PRKAR2A, MYBL1, and Trim44 and inhibits the expression of Sash1 and Smad5 via autophagy. Our observations suggest that miR-1307 promotes hepatocarcinogenesis by CALR-OSTC-endoplasmic reticulum protein folding pathway.

INTRODUCTION

Several studies have found that miR-1307 is associated with the occurrence and development of various human diseases. Zheng Yang found that miR-1307-3p was significantly downregulated in the process of cartilage differentiation (Yang et al., 2018). Balmeh et al. showed that miR-1307-3p could indirectly target type 2 diabetes gene (Balmeh et al., 2020). Takamura et al. found that miR-1307-3p could target NDRG2 and inhibit osteoclast formation (Takamura et al., 2018). There is abnormal expression of miR-1307-3p in human cardiac and peripheral adipose-derived mesenchymal stem cells (Ruan et al., 2020). In particular, miR-1307 plays a role in various cancers. Zheng et al. found that miR-1307-3p inhibited the activation of Wnt3a/β-Catenin signal, thereby inhibiting the proliferation of colon adenocarcinoma cells (Zheng et al., 2019). Su et al. confirmed that miR-1307 was upregulated in serum exosomes of ovarian cancer and proposed that miR-1307 was related to tumor stage (Su et al., 2019). Zhou et al. believe that miR-1307 may play a role in the development of chemoresistance in ovarian cancer (Zhou et al., 2015). Studies have shown that miR-1307-3p is also associated with chemotherapy-resistant ovarian cancer (Zhou et al., 2019). In conclusions, miR-1307 plays a regulatory role in a variety of diseases and tumors; however, its role in liver cancer has not been clarified.

Because of the increase of protein synthesis under environmental pressure, proteins in organelles usually fail to fold, resulting in the accumulation of misfolded proteins. And then it activates the corresponding protein response to restore homeostasis, which is called UPR (unfolded protein response) (Wang and Kaufman, 2016). UPR downstream components strictly control transcription and translation reprogramming to ensure selective gene expression (Zhao et al., 2020). The overactivation of these three pathways is associated with tumor formation (Oakes 2020). If endoplasmic reticulum stress is at a high level for a long time, UPR can promote cell self-extinction (Oakes and Papa, 2015). Cancer cells are subject to a variety of adverse factors, including gene mutation, hypoxia, and nutritional deficiency, resulting in endoplasmic reticulum stress and triggering UPR (Moenner et al., 2007). Liu et al. indicated that liver cancer cells under endoplasmic reticulum stress released exosomes to upregulate the expression of PD-L1 and then inhibit T cell function (Liu et al., 2019). Scott et al. confirmed that changing the expression of ER chaperone

[1]Shanghai Putuo People's Hospital, School of Life Science and Technology, Tongji University, 200092 Shanghai, China

[2]These authors contributed equally

[3]Lead contact

*Correspondence: ludongdong@tongji.edu.cn

https://doi.org/10.1016/j.isci.2021.103271

This is an open access article under the CC BY-NC-ND license (http://creativecommons.org/licenses/by-nc-nd/4.0/).

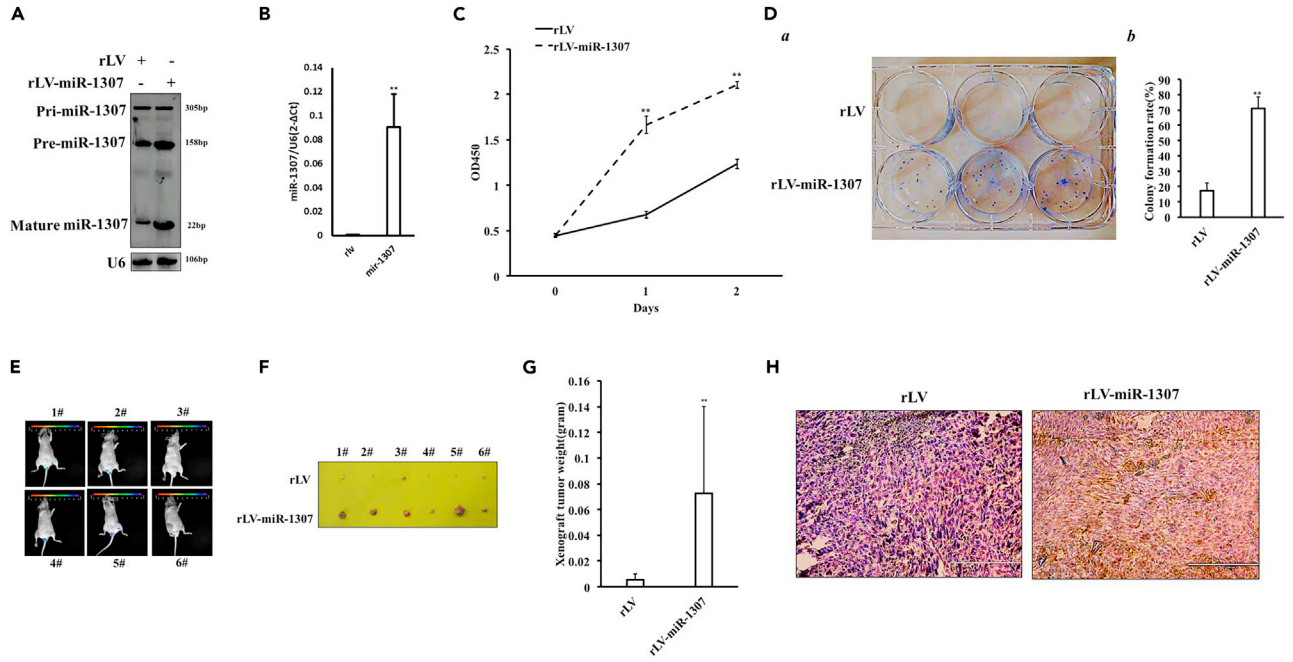

Figure 1. miR-1307 promotes the growth of liver cancer cells *in vitro* and *in vivo*

(A) Northern blotting was used to detect miR-1307 and U6.

(B) Quantitative RT-PCR was used to detect the mature miR-1307 and U6. The values of each group were expressed as mean ± SD (n = 3); * *p < 0.01, *p < 0.05.

(C) CCK8 method was used to determine the cell proliferation ability. The values of each group were expressed as mean ± SD (n = 3); * *p < 0.01, *p < 0.05.

(D) The colony forming ability of cells was measured. (a) Photos of plate colonies. (b) Analysis of colony forming ability of cells. The values of each group were expressed as mean ± standard deviation (bar ± SD, n = 3); * *p < 0.01, *p < 0.05.

(E) *In vivo* Hep3B cells were inoculated subcutaneously into BALB/C nude mice for one month.

(F) The xenograft tumor was dissected.

(G) Comparison of tumor size (g). The values of each group were expressed as mean ± SD (n = 6); * *p < 0.01, *p < 0.05 respectively.

(H) The transplanted tumor tissue sections (4 μm) were performed in anti-PCNA immunohistochemical staining (original registration × 100).

affected the growth of tumor cells (Oakes, 2017). Furthermore, UPR apoptosis pathway was induced by increasing the levels of C/EBP homologous protein (Deng et al., 2020).

In this study, our studies confirm that miR-1307 has an effect on the malignant proliferation of human liver cancer cells and reveal the effect of miR-1307 on the signal pathway network in human liver cancer cells. Importantly, this study reveals the mechanism of miR-1307 on the proliferation of liver cancer cells by affecting the folding proteins via endoplasmic reticulum and provides new ideas for the treatment of a variety of cancers.

RESULTS

miR-1307 promotes the growth of liver cancer cell *in vitro* and *in vivo*

To investigate the effect of miR-1307 on human liver cancer cells, the pre-miR-1307 (refseq: MI0006444) was cloned into pVLX-ZsGreen-miRNA-Puro (Figure S1). pLVX-Zsgreen-miR-1307-puro was packaged into a lentivirus rLV-miR-1307. The human liver cancer cell line Hep3B was infected with rLV-miR-1307. The positive cells were selected under fluorescence microscope (Figure S2A). miR-1307 precursor and mature miR-1307 were significantly increased in rLV-miR-1307 group compared with rLV group (Figures 1A, 1B, and S2B). The cell proliferation ability was significantly increased in rLV-miR-1307 group compared with rLV group (24 h: $p = 0.000000882 < 0.01$; 48 h: $p = 0.000000169 < 0.01$) (Figure 1C). The formation rate of plate colony was significantly increased in rLV-miR-1307 group compared with rLV group (29.2 ± 5.89% versus 78.4 ± 5.302%, $p = 0.008329 < 0.01$, Figure 1Da&b; 17.13 ± 5.33% versus 70.87 ± 7.52%, $p = 0.007499 < 0.01$, Figures S3A and S3B). The average weight of xenograft tumor was significantly increased in rLV-miR-1307 group compared with rLV group ($p = 0.0041057 < 0.01$) (Figures 1E–1G). HE staining

showed less high-differentiated cancer cells and more low-differentiation cells in rLV-miR-1307 group than those in rLV group (Figure S4). PCNA expression was significantly increased in rLV-miR-1307 group compared with rLV group (Figure 1H). Collectively, miR-1307 promotes growth of liver cancer cells *in vivo* and *in vivo*.

miR-1307 alters transcriptomics, proteomics, and regulatory omics of human hepatoma cells

To explore how miR-1307 affects the epigenetic regulation in human liver cancer cells, the chromatin immunoprecipitation sequencing with anti-H3K9me2 was preformed. As shown in Figure S5A, the distribution of H3K9m2 modification on 23 pairs of chromosomes was showed in rLV group and rLV-miR-1307 group. As shown in Figure S5B, the peak difference of genes between rLV group and rLV-miR-1307 group was shown, including GCLC, CFTR, WNT16, NA, CYP51A, HECW1, ICA1, KDM1A, RBM6, RAX, KDM4C, CUBN, ARX, KDM4C, CUBN1, CDC27, CALCR, CREBBP, CDK14, TRPM3, KDM4C, SNX16, etc. As shown in Figure S5C, the visualization analysis results of peak difference genes were shown in rLV group and rLV-miR-1307 group, such as, KDM4C, TBX22, UBE3C, Rad50, HDAC2, PRPC2C, CALN1, Sox5, TUT4, etc. Next, the effect of miR-1307 on transcriptome of liver cancer cells was analyzed by RNA-Seq. The analysis of Wayne diagram showed that 3,845 differential genes were overlapped in the two groups, 338 differential genes only appeared in rLV-miR-1307 group, and 585 differential genes only appeared in rRLV group (Figure S5D). Volcano map analysis showed that there were 250 upregulated and 300 downregulated genes (Figure S5E). The heat map analysis showed the differential gene classification (Figure S5F), and the downregulated genes mainly included OSTC, ARF5, LMNA, ATAD2, RSP5, UBE2M, CAPZB, MCM5, THRA, CKS1B, HBP1, TUBA1C, EFNB2, KDM3A, CCT3, OTUB1, RPLP1, CCNA2, ELAVL2, MARCKS, TUBB, etc., and the down regulated genes mainly included LMNA, CALR, TUBA1C, CCT3, CAPZB, MCM5, CKSB1, TUBAC, CCT3, CCNA2, ELAVL2, MARCKS, TUBB, ATP8B2, PPIG, CALR, TPM3, SF3B3, CAP1, NAA15, SCAF1, TPM3, PSIP1, NAA15, GMPS, SCAF1, PSIP1, GMPS, HOXA5, UBAP2L, TUBA1B, MCM4, TOP2A, PRCC, PHF6, ASAP1, EHD3, etc.

The effect of miR-1307 on the proteomics of liver cancer cells was analyzed by label-free quantitative proteomics assay. Differential protein volcano map showed that 208 genes were upregulated and 227 genes were downregulated in 3,335 proteins (Figure S5G). Upregulated proteins mainly include TOP2A, LPR1, RAB7A, CALU, SP1, CAVIN1, DLD, Rad21, CTCF, JUN, HSPG2, HIST1H2A, CBX, PRKAR, PPP1R7, CAVIN3, CARMIL, FOXP4, PRKAR, TBK1, FAM20B, DNMT3A, and CDK2AP1, and downregulated proteins mainly include TUBA1C, TUBB4A, PHB, XPO1, EIF5A, EIF3D, KAT7, PFKL, OGT, MTOR, PFKM, DTBP3, EIF2A, CDC16, TFAD4, CARM1, UBE4B, CCDCB4, BIN1, EIF3H, SETDB1, PPKCD, and UBASH3B.The interaction molecular network of the endoplasmic reticulum (ER) regulatory factor CALR was revealed by immunoprecipitation with anti-CALR-mass spectrometry analysis. The total CALR binding proteins were analyzed by 10% SDS-PAGE electrophoresis (Figure S5H). Cluster analysis (Figure S5I) and volcano map (Figure S5J) showed the CALR binding differential protein level, including 168 upregulated proteins and 100 downregulated proteins), e.g. MYH10, TPM3, ENO3, ACLY, DDB1, CALD1, SEC233A, AP2S1, TXN, DDOST, AARS, ETF1, SDTBN1, etc. CALR binding proteins in two groups were analyzed by domain enrichment analysis. The types and distribution of domains (Figure S5K) and the enriched domain bubble (Figure S5L) were plotted. It mainly includes HistoneH3, Histone H4, HistoneH2B, SNF2, bromodomain, Tudor domain, Sec63 domain, CRF1 domain, MTRA, soluble ligand binding domain, nucleic acid binding, CARM1 N terminal domain, SecY/SEC61-alpha, histone-fold domain, SH2 domain, zinc-finger domain, coatomer domain, protein kinase domain, 26S proteasome 2B, and catalytic subunit beta. CALR binding proteins were analyzed by using the StringDB protein interaction database, and the network diagram was constructed (Figure S5M). Collectively, these observations suggest that miR-1307 alters transcriptomics, proteomics, and regulatory omics in human liver cancer cells.

miR-1307 inhibits the expression of METTL8

To investigate the effect of miR-1307 on the expression of METTL8, KDM3A, and KDM3B in human liver cancer cell, firstly, human liver cancer cell line Hep3B was infected with rLV-miR-1307 and rLV, respectively (Figure S6). Both miR-1307 precursor and mature miR-1307 were significantly increased in rLV-miR-1307 group compared with rLV group (Figures 2A and 2B). Bioinformatics analysis shows that the mature sequence of miR-1307 binds to the 3′-noncoding region (2225-2232) of METTL8 mRNA through eight-base seed sequence (Figure 2C). The activity of pMirTarget-METTL8 3′-UTR-Luc reporter gene was significantly decreased in rLV-miR-1307 group compared with rLV group (21072.26 $\pm$ 3042.79 versus 6421.82 $\pm$ 1053.43, $p = 0.00592 < 0.01$) (Figure 2D). The activity of pMirtarget-METTL8 3′-UTR(mutant)-Luc reporter gene was not altered in rLV-miR-1307 group compared with rLV group (27,622.08 $\pm$ 6506.36 versus

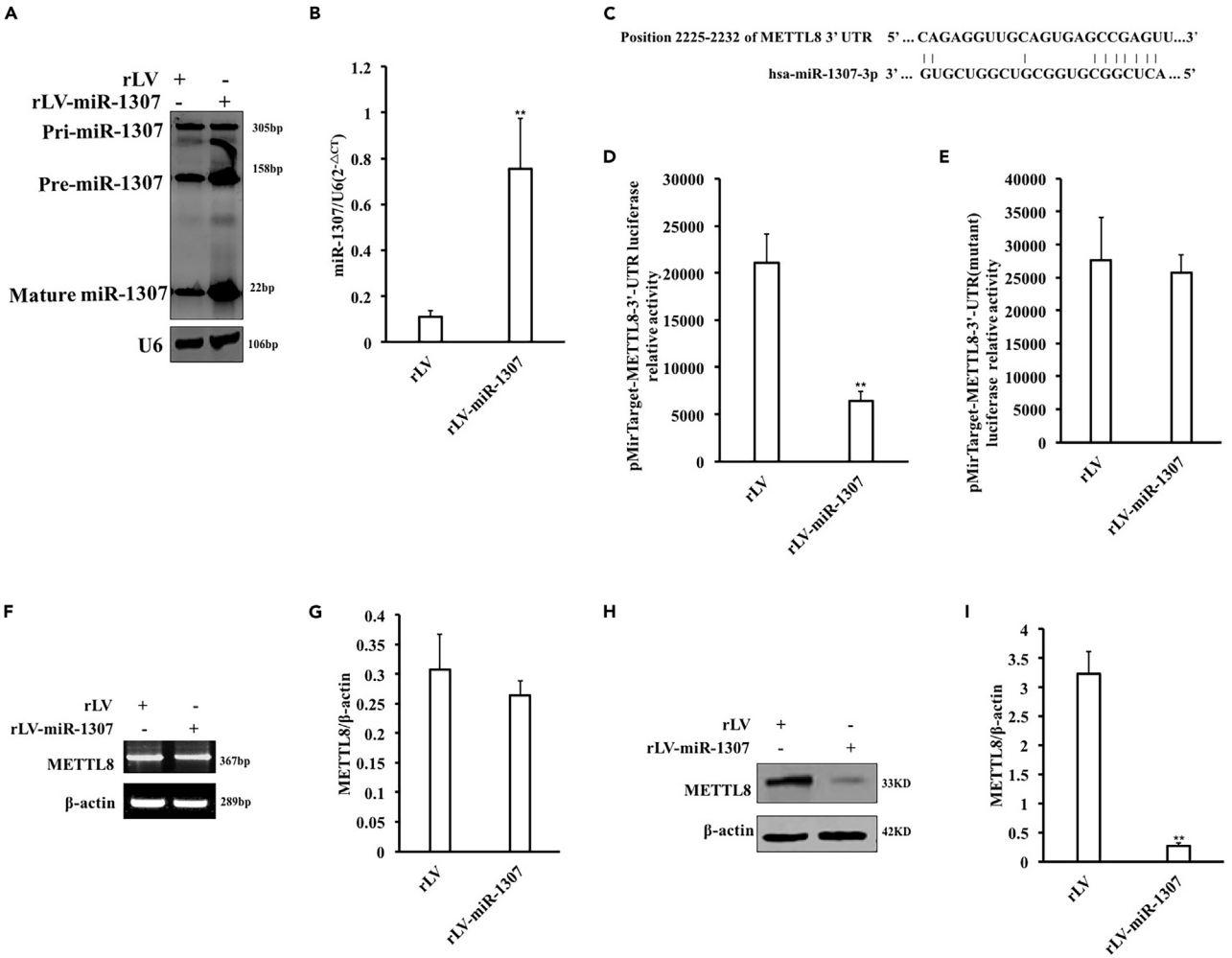

Figure 2. miR-1307 targets METTL8 and inhibits METTL8 expression

(A) Total RNA was extracted, and northern blotting was used to detect miR-1307. U6 as internal reference genes.

(B) qRT-PCR was used to detect the mature miR-1307. Each experiment was repeated three times. The values of each group were expressed as mean ± SD (n = 3); * *p < 0.01, *p < 0.05.

(C) Bioinformatics was used to analyze the seed sequence of mature miR-1307 binding to 3′UTR of METTL8 mRNA.

(D) The activity of pMirtarget-METTL8 3′-UTR-Luc reporter gene was detected. Each experiment was repeated three times. The values of each group were expressed as mean ± SD (n = 3); * *p < 0.01, *p < 0.05.

(E) The activity of pMirtarget-METTL8 3′ UTR(mutant) Luc reporter gene.

(F) RT-PCR was used to detect METTL8. β-actin was used as the internal reference gene.

(G) Quantitative RT-PCR analysis. Each experiment was repeated three times. The values of each group were expressed as mean ± SD (n = 3); * *p < 0.01, *p < 0.05.

(H) Western blotting was used to detect METTL8. β-actin was used as internal reference gene.

(I) Gray scan analysis of positive bands. Each experiment was repeated three times. The values of each group were expressed as mean ± SD (n = 3); * *p < 0.01, *p < 0.05.

25752.34 ± 2690.37, p = 0.3783 > 0.05) (Figure 2E). Although METTL8 mRNA was not changed in rLV-miR-1307 group compared with rLV group (Figures 2F and 2G), METTL8 protein was significantly decreased in rLV-miR-1307 group compared with rLV group (Figures 2H and 2I). Collectively, these results suggest that miR-1307 targets METTL8 3′UTR and inhibits the expression of METTL8 in liver cancer cells.

miR-1307 inhibits KDM3A and KDM3B by reducing METTL8

In view of the inhibition of the expression of METTL8 via miR-1307 in human liver cancer cells, we will analyze whether miR-1307 affects the expression of KDM3A and KDM3B by reducing METTL8. RIP-seq

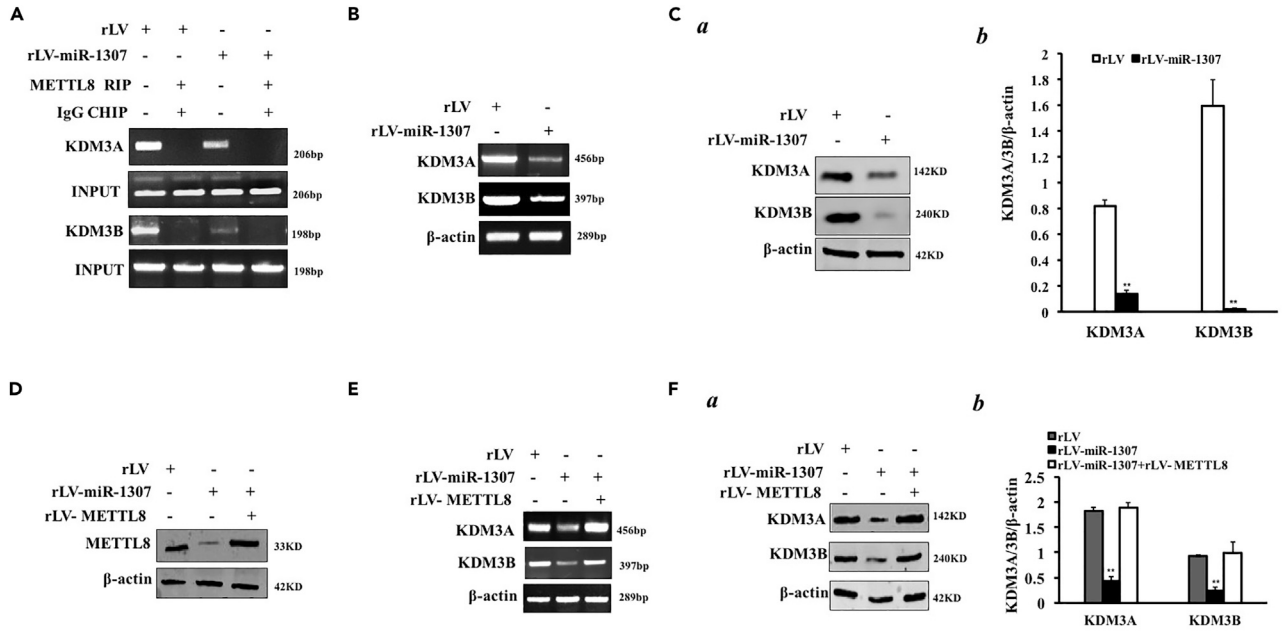

Figure 3. miR-1307 inhibits the expression of KDM3A and KDM3B by reducing METTL8 in liver cancer cells

(A) RNA immunoprecipitation (RIP) with anti-METTL8 was performed. RT-PCR was used to detect KDM3A and KDM3B mRNA. IgG RNA immunoprecipitation was used as negative control.

(B) RT-PCR was used to detect KDM3A and KDM3B. β-actin was used as internal reference gene.

(C) (a) The total protein was extracted, and the expression of KDM3A and KDM3B was detected by western blotting. β-actin was used as the internal reference gene. (b) Gray scan analysis of positive bands. Each experiment was repeated three times. The values of each group were expressed as mean ± SD (n = 3); * *p < 0.01, *p < 0.05.

(D) The expression of METTL8 was analyzed by western blot. β-actin was used as the internal reference gene.

(E) RT-PCR was used to detect KDM3A and KDM3B. β-actin was used as internal reference gene.

(F) (a) The expression of KDM3A and KDM3B was detected by western blotting. β-actin was used as the internal reference gene. (b) Gray scan analysis of positive bands.

analysis showed that the binding ability of METTL8 with KDM3A mRNA, KDM3B mRNA, OGT mRNA, CDC16 mRNA, CARM mRNA, and SETDB1 mRNA was significantly decreased, and the binding ability of METTL8 with JUN mRNA, FOXP4 mRNA, CDKAP1 mRNA, PRKAR mRNA, and PPP1R7 mRNA was significantly increased in rLV-miR-1307 group compared with rLV group (Figures 3A, S7A and S7B). Thereby, the KDM3A and KDM3B mRNA were significantly reduced in rLV-miR-1307 group compared with rLV group (Figure 3B), and the translational ability of KDM3A and KDM3B was significantly reduced in rLV-miR-1307 group compared with rLV group (Figure 3Ca&b). The expression of METTL8 was significantly decreased in rLV-miR1307 group compared with rLV group and increased in rLV-miR-1307 + rLV-METTL8 group (Figure 3D). Although the KDM3A mRNA and KDM3B mRNA were significantly reduced in rLV-miR-1307 group compared with rLV group, it was not significantly altered in rLV-miR-1307+rLV-METTL8 group compared with rLV group (Figure 3E). Although the expression of KDM3A and KDM3B were significantly reduced in rLV-miR-1307 group compared with rLV group, it was not significantly altered in rLV-miR-1307+rLV-METTL8 group compared with rLV group (Figure 3Fa&b). Collectively, these results suggest that miR-1307 inhibits the expression of KDM3A and KDM3B by reducing METTL8 in liver cancer cells.

miR-1307 increases the methylation of histone H3 lysine 9 by inhibiting the expression of KDM3A and KDM3B

Given that miR-1307 inhibits the expression of KDM3A and KDM3B in human liver cancer cells, we will analyze whether miR-1307 affects the methylation modification of histone H3 at the ninth lysine by inhibiting KDM3A and KDM3B. First, protein immunoprecipitation (IP) analysis showed that the binding ability of histone H3 to KDM3A and KDM3B was significantly decreased in rLV-miR-1307 group compared with rLV group (Figure 4A). Although the methylation of histone H3 at the ninth lysine (H3K9me1, H3K9me2, H3K9me3) was significantly increased in rLV-miR-1307 group compared with rLV group, it was not

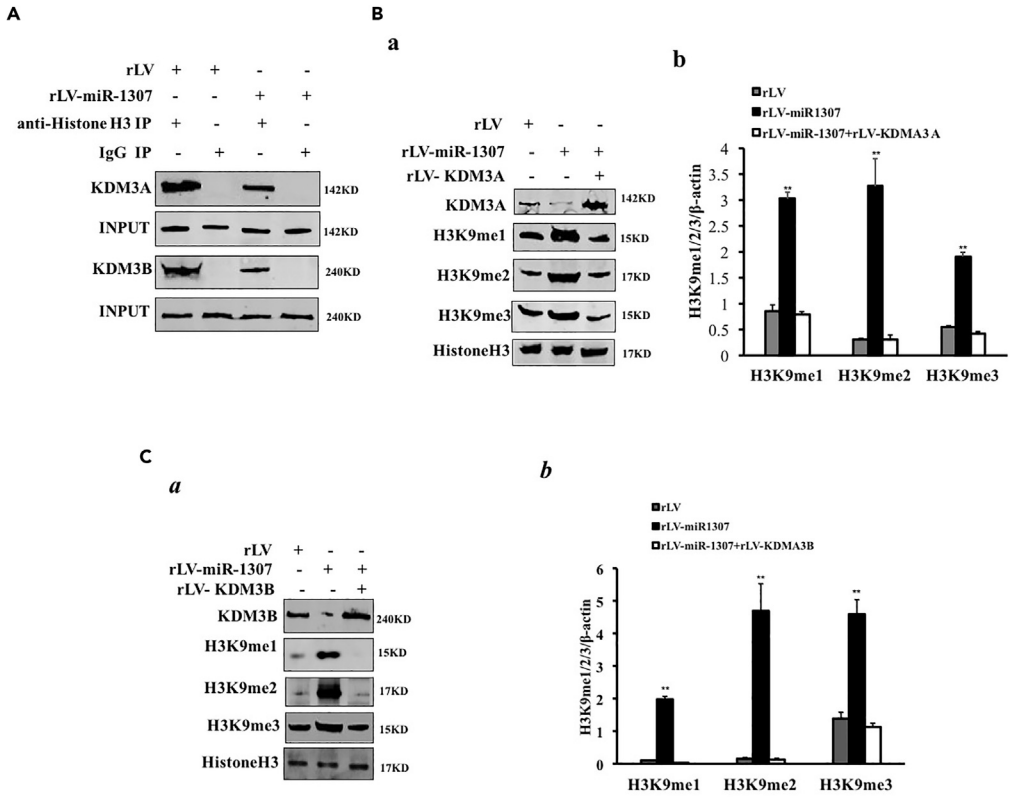

Figure 4. miR-1307 increases the methylation of histone H3 at the ninth lysine

(A) The samples were co-precipitated with anti-histone H3, and the precipitates were analyzed by western blotting with anti-KDM3A and anti-KDM3B. IgG immunoprecipitation was used as negative control.

(B) (a) Western blotting analysis was performed with anti-K3K9me1, anti-H3K9me2, and anti-H3K9me3. Histone H3 was used as the internal reference gene. (b) Gray scan analysis of positive bands. Each experiment was repeated three times. The values of each group were expressed as mean ± SEM (n = 3); * *p < 0.01, *p < 0.05.

(C) (a) Western blotting analysis was performed with anti-K3K9me1, anti-H3K9me2, and anti-H3K9me3. Histone H3 was used as the internal reference gene. (b) Gray scan analysis of positive bands. Each experiment was repeated three times. The values of each group were expressed as mean ± SD (n = 3); * *p < 0.01, *p < 0.05.

significantly changed in rLV-miR-1307 + rLV-KDM3A group compared with rLV group (Figure 4Ba&b). Although the methylation of histone H3 at the ninth lysine (H3K9me1, H3K9me2, H3K9me3) was significantly increased in rLV-miR-1307 group compared with rLV group, it was not significantly changed in rLV-miR-1307+rLV-KDM3B group compared with rLV group (Figure 4Ca&b). Collectively, these results suggest that miR-1307 increases the methylation of histone H3 at the ninth lysine by inhibiting the expression of KDM3A and KDM3B.

miR-1307 promotes the expression of endoplasmic reticulum regulatory protein CALR via H3K9me2

Because miR-1307 increases methylation on the ninth lysine of Histone H3 by inhibiting the expression of KDM3A and KDM3B, we will analyze whether miR-1307 alters the expression of CALR in liver cancer cells by H3K9me2. First, the binding ability of H3K9me2 and RNA polII to the promoter region of CALR was significantly increased in rLV-miR-1307 group compared with rLV group (Figure 5A). Although the methylation of histone H3 at the ninth lysine (H3K9me1, H3K9me2, H3K9me3) was significantly increased in rLV-miR-1307 group compared with rLV group, it was not significantly changed in rLV-miR-1307 + BIX-01294 group (BIX-01294 is the specific inhibitor of H3K9me2) (Figure 5B). The binding ability of H3K9me2, P300, and RNA polII to the promoter region of CALR was significantly increased in rLV-miR-1307 group compared with rLV group; it was not significantly changed in rLV-miR-1307+BIX-01294 group (Figure 5C). The binding ability of CALR promoter probe to H3K9me2 was significantly increased in rLV-miR-1307 group compared with rLV group; it was not significantly changed in rLV-miR-1307+BIX-01294 (Figure 5D). The binding ability of CALR

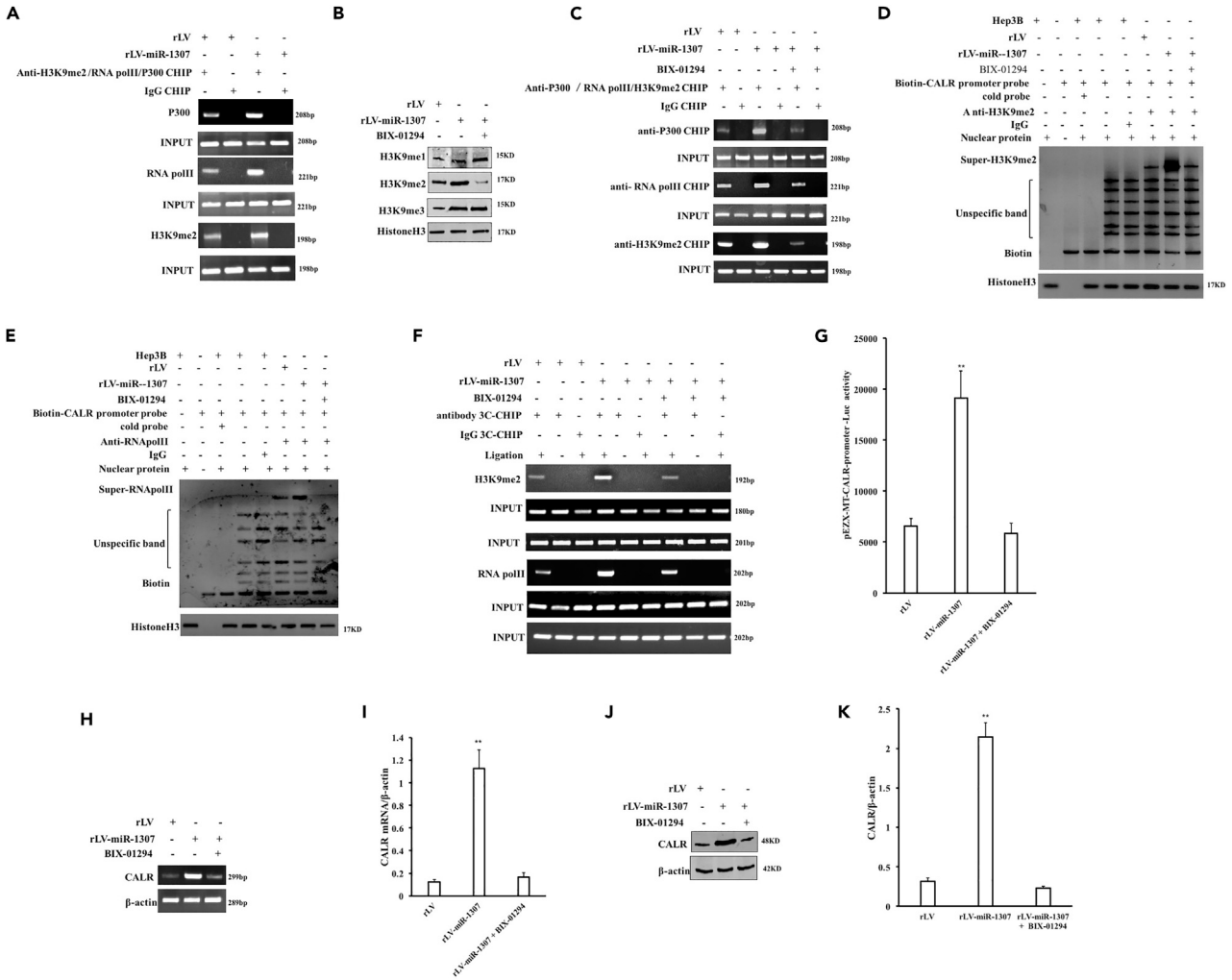

Figure 5. miR-1307 enhances the expression of CALR by depending on H3K9me2

(A) Chromatin immunocoprecipitation (CHIP) analysis was performed by anti-H3K9me2 and anti-RNA polII, respectively. The PCR amplification was performed by using primers designed according to the DNA of CALR promoter region. IgG CHIP was used as the negative control.

(B) The western blotting was performed by using anti-H3K9me1, anti-H3K9me2, and anti-H3K9me3. Histone H3 was used as the internal reference gene.

(C) The CHIP analysis was performed by anti-H3K9me2 and anti RNA polII, respectively. The PCR amplification was carried out by using primers designed according to the DNA of CALR promoter region. IgG chip was used as the negative control.

(D) Super-EMSA with CALR promoter probe labeled with biotin (Biotin-CALR) and anti-H3K9me2 and anti-Biotin was performed.

(E) Super-EMSA with CALR promoter probe labeled with biotin (Biotin-CALR) and anti-RNApolII and anti-Biotin was performed.

(F) The binding ability of H3K9me2 and RNApolII with the promoter-enhancer loop of CALR was analyzed by the chromosome configuration capture (3C)-chromatin immunocoprecipitation (chip).

(G) pEZX-MT-CALR-promoter-Luc activity was detected. Each experiment was repeated three times. The values of each group were expressed as mean ± SEM (n = 3); * *p < 0.01, *p < 0.05.

(H) The transcription ability of CALR was detected by RT-PCR. β-actin was used as the internal reference gene.

(I) Quantitative RT-PCR analysis. Each experiment was repeated three times. The values of each group were mean ± SD (n = 3); * *p < 0.01, *p < 0.05.

(J) The translation ability of CALR was detected by western blotting. β-actin was used as the internal reference gene.

(K) Gray scan analysis of positive strip. Each experiment was repeated three times. The values of each group were mean ± SD (n = 3); * *p < 0.01, *p < 0.05.

promoter probe to RNApolII was significantly increased in rLV-miR-1307 group compared with rLV group; it was not significantly changed in rLV-miR-1307 + BIX-01294 (Figure 5E). The binding ability of H3K9me2 and RNApolII to CALR promoter-enhancer loop was significantly increased in rLV-miR-1307 group compared with rLV group; it was not significantly changed in rLV-miR-1307 + BIX-01294 (Figure 5G). Although the CALR promoter luciferase reporter gene activity was significantly increased in rLV-miR-1307 group compared with rLV group (6560.85 ± 773.42 versus 19,112.77 ± 2644.07, p = 0.005134 < 0.01), it was

not significantly changed in rLV-miR-1307+BIX-01294 (6560.85 ± 773.42 versus 5870.86 ± 970.68, $p = 0.1041 > 0.05$) (Figure 5F). Finally, the transcriptional level of CALR was significantly increased in rLV-miR-1307 group compared with rLV group; it was not significantly changed in rLV-miR-1307+BIX-01294 (Figures 5H and 5I). The expression of CALR was significantly increased in rLV-miR-1307 group compared with rLV group; it was not significantly changed in rLV-miR-1307 + BIX-01294 compared with rLV group (Figures 5J and 5K). Collectively, these results suggest that miR-1307 enhances the expression of CALR by depending on H3K9me2.

miR-1307 alters cyclins via the CALR-OSTC-protein folding pathway

Because miR-1307 promotes the expression of CALR and inhibits the expression of OSTC, we will analyze whether miR-1307 changes cyclins expression and its interaction via the CALR-OSTC endoplasmic reticulum protein folding pathway in liver cancer. First, co-immunoprecipitation (IP) analysis showed that the binding ability of OSTC to CDK2, CDK4, CyclinD1, and cyclinE was significantly decreased in rLV-miR-1307 group compared with rLV group (Figure 6A). The binding ability of CALR to CDK2, CDK4, CyclinD1, and cyclinE was significantly enhanced in rLV-miR-1307 group compared with rLV group (Figure 6B). Although the interaction between CDK2 and cyclinE was significantly increased in rLV-miR-1307 group compared with rLV group, it was not significantly altered in rLV-miR-1307 + silibinin (protein misfolding inhibitor) group compared with rLV group (Figure 6C). Although the interaction between CDK4 and CyclinD1 was significantly increased in rLV-miR-1307 group compared with rLV group, it was not significantly altered in rLV-miR-1307 + silibinin (protein misfolding inhibitor) group compared with rLV group (Figure 6D). Finally, although the expressions of p21WAF1/CIP1, GADD45, pRB, and P18 were significantly decreased and the expressions of ppRB and PCNA were significantly increased in rLV-miR-1307 group compared with rLV group, it was not significantly altered in rLV-miR-1307 + silibinin group compared with rLV group (Figure 6E). Collectively, these results suggest that miR-1307 alters the expression of cyclins p21WAF1/CIP1, GADD45, P18, pRB, ppRB, and PCNA by CALR-OSTC-protein folding pathway.

miR-1307 enhances the activity of H-ras, PKM2, and PLK1 via the CALR-OSTC-protein folding pathway

Given that miR-1307 promotes the expression of CALR and inhibits the expression of OSTC, we will analyze whether miR-1307 alters the activities of H-ras, PKM2, and PLK1 via the CALR-OSTC-protein folding pathway. First, protein immunoprecipitation (IP) analysis showed that the binding ability of OSTC to H-Ras, PKM2, and PLK1 was significantly decreased in rLV-miR-1307 group compared with rLV group (Figure 7A). The binding ability of CALR to H-Ras, PKM2, and PLK1 was significantly enhanced in rLV-miR-1307 group compared with rLV group (Figure 7B). The activity of H-ras was significantly increased in rLV-miR-1307 group compared with rLV group; it was not significantly altered in rLV-miR-1307 + silibinin group compared with rLV group (Figures 7C and 7D). Although the expression of PKM2 was significantly increased in rLV-miR-1307 group compared with rLV group, it was not significantly altered in rLV-miR-1307 + silibinin group compared with rLV group (Figure 7E). The activity of PKM2 was significantly increased in rLV-miR-1307 group compared with rLV group (GlycoPER:2.25 ± 0.37 versus 8.62 ± 0.58, $p = 0.00036 < 0.01$; NAD+: 0.57 ± 0.08 versus 1.14 ± 0.62, $p = 0.0084 < 0.01$); it was not significantly altered in rLV-miR-1307 + silibinin group compared with rLV group (GlycoPER:2.25 ± 0.37 versus 3.00 ± 0.85, $p = 0.129 > 0.05$; NAD+: 0.57 ± 0.08 versus 0.59 ± 0.11, $p = 0.295 > 0.05$) (Figures 7F and 7G). The expression of PLK1 and PKG in rLV-miR-1307 group was significantly increased in rLV-miR-1307 group compared with rLV group; it was not significantly altered in rLV-miR-1307 + silibinin group compared with rLV group (Figure 7H). The PLK1 activity was significantly increased in rLV-miR-1307 group compared with rLV group (0.31 ± 0.08 versus 0.93 ± 0.06, $p = 0.00019 < 0.01$); it was not significantly altered in rLV-miR-1307 + silibinin group compared with rLV group (0.31 ± 0.08 versus 0.34 ± 0.11, $p = 0.382 > 0.05$) (Figure 7I). Collectively, these results suggest that miR-1307 enhances the activities of H-ras, PKM2, and PLK1 via the CALR-OSTC-protein folding pathway.

miR-1307 inhibits autophagy and promotes the expression of oncogene dependent on the endoplasmic reticulum protein folding pathway

Given that miR-1307 enhances the expression of CALR and inhibits the expression of OSTC, we will analyze whether miR-1307 inhibits autophagy and promotes the expression of oncogene dependent on the endoplasmic reticulum protein folding pathway in liver cancer cells. The binding ability of OSTC with ATG4 was significantly decreased in rLV-miR-1307 group compared with rLV group (Figure 8A). The binding ability of CALR with ATG4 was significantly increased in rLV-miR-1307 group compared with rLV group (Figure 8B). Although the binding ability of ATG4 with LC3 was significantly decreased in rLV-miR-1307 group

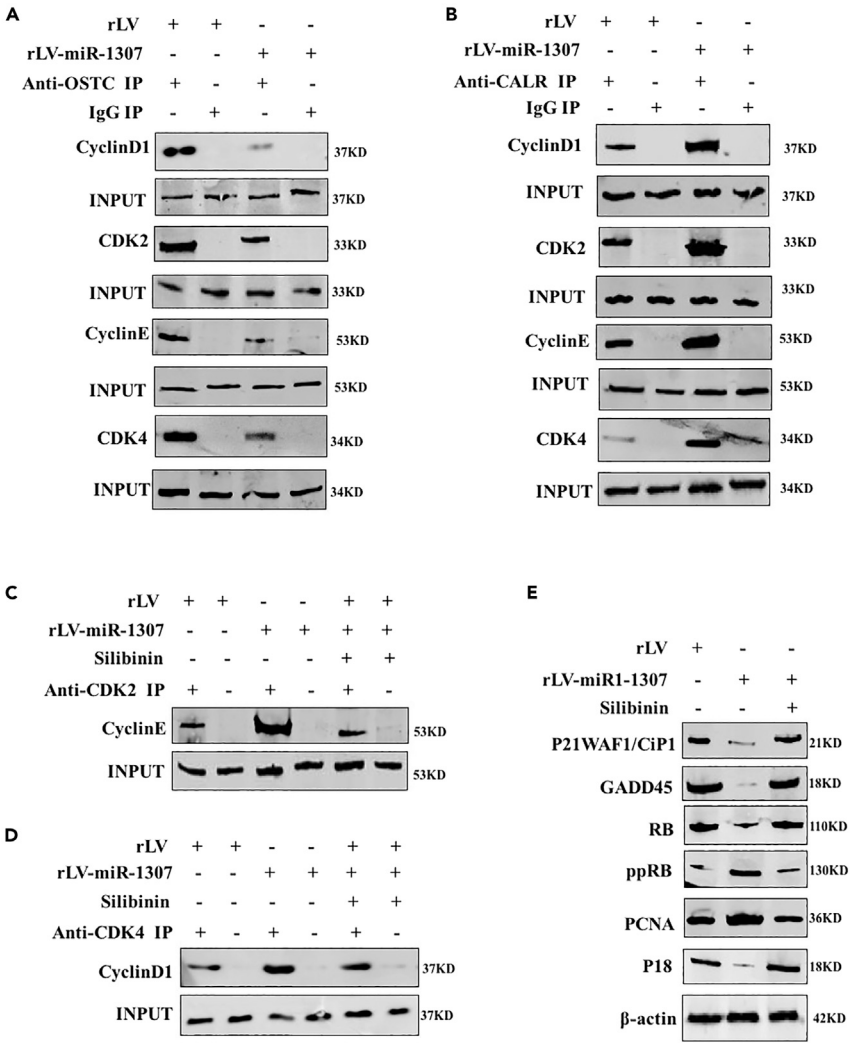

Figure 6. miR-1307 alters the expression of cyclins by CALR-OSTC-protein folding pathway

(A) The total proteins were extracted and analyzed by co-immunoprecipitation (IP). The samples were immunoprecipitated with anti-OSTC, and the precipitates were analyzed by western blotting with anti-CDK2, anti-CDK4, anti CyclinD1, and anti-cyclinE. IgG immunoprecipitation was used as negative control. Western blotting was used to detect anti-OSTC as input.

(B) The total protein was extracted and analyzed by co-immunoprecipitation (IP). The samples were immunoprecipitated by anti-CALR, and the precipitates were analyzed by western blotting with anti-CDK2, anti-CDK4, anti CyclinD1, and anti-cyclinE. IgG co-immunoprecipitation was used as negative control.

(C) Total proteins were extracted and analyzed by co-immunoprecipitation (IP). The samples were co-precipitated with anti-CDK2, and the precipitates were analyzed by western blotting with anti-cyclinE.

(D) Total proteins were extracted and analyzed by immunoprecipitation (IP). The samples were co-precipitated with anti-CDK4, and the precipitates were analyzed by western blotting with anti-cyclinD1.

(E) Western blotting analysis was performed with anti-p21waf1/CIP1, anti-GADD45, anti-p18, anti-pRB, anti-ppRB, and anti-PCNA. β-actin was used as the internal reference gene.

compared with rLV group, it was not significantly altered in rLV-miR-1307 + silibinin group compared with rLV group (Figure 8C). Although the active LC3II was significantly reduced in rLV-miR-1307 group compared with rLV group, it was not significantly altered in rLV-miR-1307 + silibinin group compared with rLV group (Figure 8D). Although the binding ability of LC3 with ATG3 and ATG7 was significantly reduced in rLV-miR-1307 group compared with rLV group, it was not significantly altered in rLV-miR-1307+silibinin group compared with rLV group (Figure 8E). Although the binding ability of ATG5 with ATG16L1, ATG12, ATG9, and ATG7 was significantly decreased in rLV-miR-1307 group compared with

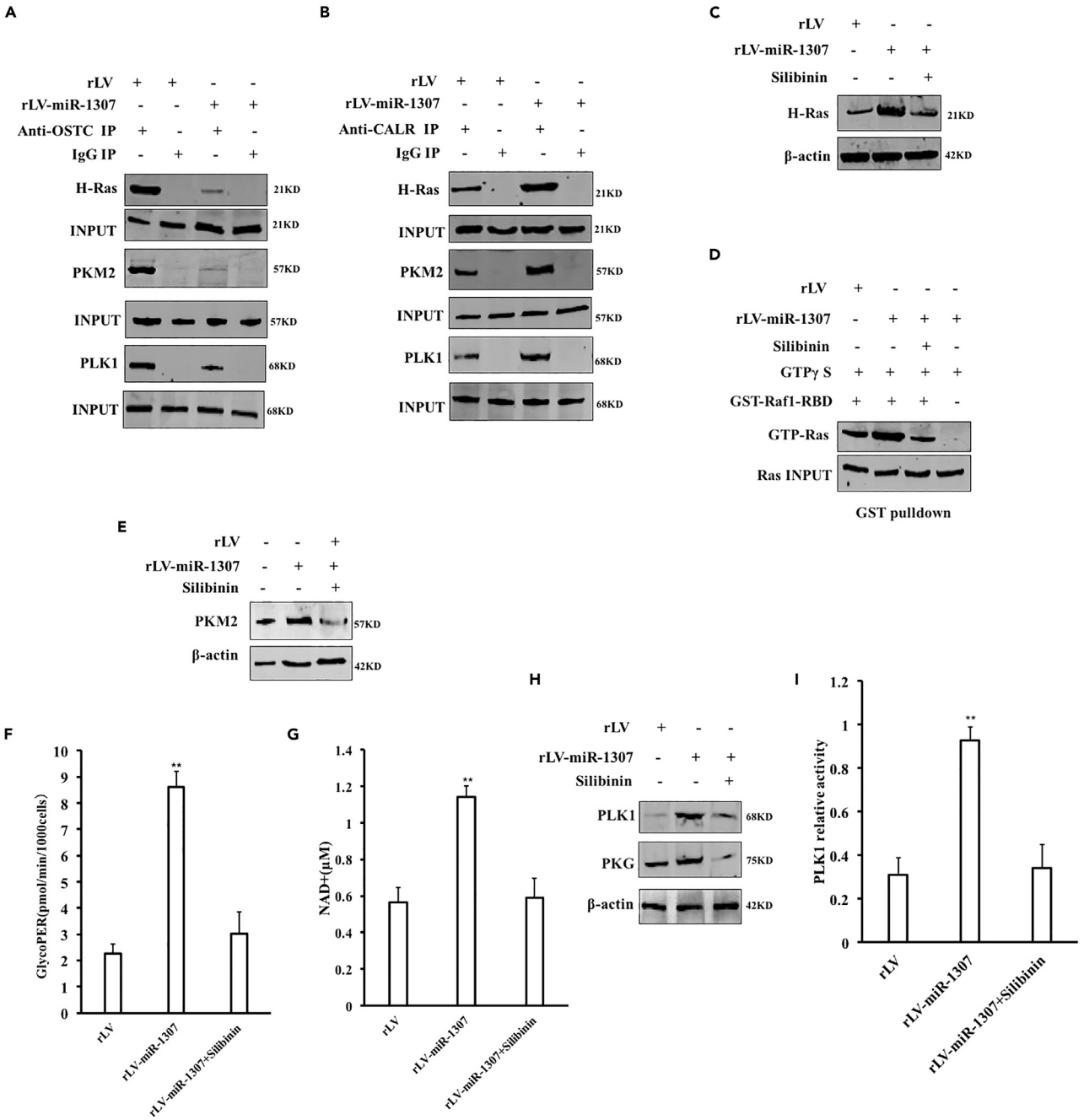

Figure 7. miR-1307 enhances the activities of H-ras, PKM2, and PLK1 via the CALR-OSTC-protein folding pathway

(A) The total protein was extracted and analyzed by immunoprecipitation (IP). The samples were co-immunoprecipitated with anti-OSTC, and the precipitates were analyzed by western blotting with anti-H-Ras, anti-PKM2, and anti-PLK1. IgG immunoprecipitation was used as negative control.

(B) The samples were co-immunoprecipitated with anti-CALR, and the precipitates were analyzed by western blotting with anti-H-Ras, anti-PKM2, and anti-PLK1.

(C) The expression of H-ras was analyzed by western blot. β-actin was used as the internal reference gene.

(D) The activity of H-ras was analyzed. The total protein was extracted, and then anti-GST was used for GST pull-down analysis.

(E) The expression of PKM2 was analyzed by western blot. β-actin was used as the internal reference gene.

(F) The activity of PM2 was analyzed. Each experiment was repeated three times. The values of each group were expressed as mean ± SEM (n = 3); * *$p < 0.01$, *$p < 0.05$.

(G) The activity of PKM22 (NAD +) was analyzed. Each experiment was repeated three times. The values of each group were expressed as mean ± SD (n = 3); * *$p < 0.01$, *$p < 0.05$.

Figure 7. *Continued*

(H) The expression of PLK1 and PKG was analyzed by western blot. β-actin was used as the internal reference gene.

(I) PLK1 kinase activity was analyzed by cell Plk1 kinase activity quantitative detection kit. Each experiment was repeated three times. The values of each group were expressed as mean ± SEM (n = 3); * *p < 0.01, *p < 0.05.

rLV group, it was not significantly altered in rLV-miR-1307 + silibinin group compared with rLV group (Figure 8F). Although the expression of Beclin1 was significantly decreased in rLV-miR-1307 group compared with rLV group, it was not significantly altered in rLV-miR-1307 + silibinin group compared with rLV group (Figure 8G). In autophagy LC3 HiBiT-reporter assay (the autophagy rate was inversely proportional to LC3 HiBiT-reporter value), although the autophagy rate was significantly reduced in rLV-miR-1307 group compared with rLV group (52.26 ± 11.0 versus 319.59 ± 23.77.p = 0.000404 < 0.01), it was not significantly altered in rLV-miR-1307 + silibinin group compared with rLV group (52.26 ± 11.0 versus 66.53 ± 19.24.p = 0.208 > 0.05) (Figure 8H). Although the incidence rate of autophagy was significantly reduced in rLV-miR-1307 group compared with rLV group (13.15 ± 1.59% versus 2.15 ± 0.81%, p = 0.00085 < 0.01), it was not significantly altered in rLV-miR-1307 + silibinin group compared with rLV group (13.15 ± 1.59% versus 11.64 ± 3.34%, p = 0.233 > 0.05) (Figure 8Ia&b). Although the expressions of PAK2, PLK1, PRKAR2A, MYBL1, and Tim44 were significantly increased and the expressions of Sash1 and Smad5 were decreased in rLV-miR-1307 group compared with rLV group, it was not significantly altered in rLV-miR-1307 + SMER28(autophagy activator) group compared with rLV group (Figure 8J). Although the expressions of PAK2, PLK1, PRKAR2A, MYBL1, and Tim44 were significantly increased and the expressions of Sash1 and Smad5 were decreased in rLV-miR-1307 group compared with rLV group, it was not significantly altered in rLV-miR-1307 + Flubendazole (autophagy activator) group compared with rLV group (Figure 8K). Collectively, these results suggest that miR-1307 inhibits autophagy and promotes the expression of oncogene dependent on the endoplasmic reticulum protein folding pathway.

Both CALR knockdown and excessive OSTC abrogate the carcinogenic function of miR-1307 in liver cancer

Given that miR-1307 inhibits autophagy and promotes the expression of oncogene dependent on the CALR-OSTC-endoplasmic reticulum protein folding pathway, we will analyze whether both CALR knockdown and excessive OSTC influence the carcinogenic function of miR-1307 in liver cancer. miR-1307 precursor and mature miR-1307 were significantly increased in rLV-miR-1307 group, rLV-miR-1307 + pGFP-V-RS-CALR group, rLV-miR-1307 + rLV-OSTC group compared with rLV group, respectively (Figures 9A and 9B). CALR was significantly increased in rLV-miR-1307 group and rLV-miR-1307 + rLV-OSTC group and decreased in rLV-miR-1307 + pGFP-V-RS-CALR group compared with rLV group, respectively. OSTC was significantly decreased in rLV-miR-1307 group and rLV-miR-1307 + pGFP-V-RS-CALR group and increased in rLV-miR-1307 + rLV-OSTC group compared with rLV group, respectively (Figure 9C). Although the proliferation ability was significantly increased in rLV-miR-1307 group compared with rLV group (24 h: p < 0.01; 48 h: p < 0.01), it was not significantly altered in rLV-miR-1307 +pGFP-V-RS-CALR group, rLV-miR-1307 + rLV-OSTC group compared with rLV group, respectively (24 h: P > 0.05; 48 h: P > 0.05) (Figure 9D). Although the colony formation ability was significantly increased in rLV-miR-1307 group compared with rLV group (30.59 ± 3.50% versus 62.01 ± 5.58%, p = 0.001 < 0.01), it was not significantly altered in rLV-miR-1307+pGFP-V-RS-CALR group, rLV-miR-1307 + rLV-OSTC group compared with rLV group, respectively (30.59 ± 3.50% versus 26.33 ± 2.32%, p = 0.1196 > 0.05; 30.59 ± 3.50% versus 33.41 ± 9.01%, p = 0.331 > 0.05) (Figure 9E). Although the average weight of xenograft tumor was significantly increased in rLV-miR-1307 group compared with rLV group (0.409 ± 0.104 g versus 0.953 ± 0.121 g, p = 0.0000000086 < 0.01), it was not significantly altered in rLV-miR-1307 +pGFP-V-RS-CALR group, rLV-miR-1307 + rLV-OSTC group compared with rLV group, respectively (0.409 ± 0.104 g versus 0.331 ± 0.144 g, P > 0.01; 0.409 ± 0.104 g versus 0.378 ± 0.046 g, p = 0.21727 > 0.05) (Figure 9G). Although the average appearance time of xenograft tumor was significantly decreased in rLV-miR-1307 group compared with rLV group (10.5 ± 1.9 days versus 6.3 ± 1.06 days, p = 0.0000679 < 0.01), it was not significantly altered in rLV-miR-1307 +pGFP-V-RS-CALR group, rLV-miR-1307 +rLV-OSTC group compared with rLV group, respectively (10.5 ± 1.9 days versus 9.3 ± 1.77 days, P > 0.05; 10.5 ± 1.9 days versus 9.8 ± 2.25 days, p = 0.128 > 0.05) (Figure 9H). Although the poorly differentiated tumor cells were significantly decreased in rLV-miR-1307 group compared with rLV group, it was not significantly altered in rLV-miR-1307+pGFP-V-RS-CALR group, rLV-miR-1307+rLV-OSTC group compared with rLV group, respectively (Figure S8A). The expression of PCNA was significantly decreased in rLV-miR-1307 group compared with rLV group; it was not significantly altered in rLV-miR-1307+pGFP-V-RS-CALR group, rLV-miR-1307+rLV-OSTC group

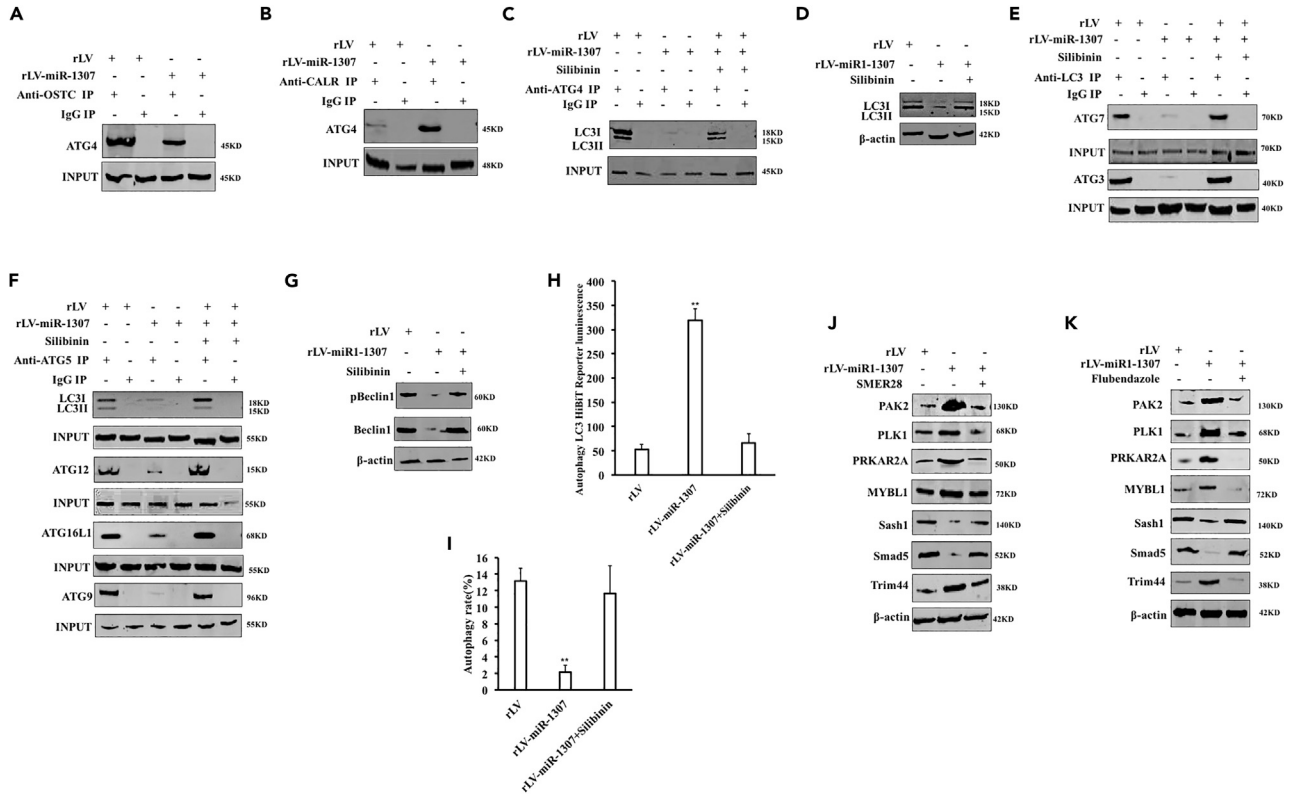

Figure 8. miR-1307 inhibits autophagy and promotes the expression of oncogene dependent on the endoplasmic reticulum protein folding pathway

(A) The total protein was extracted and analyzed by immunoprecipitation (IP). The samples were co-precipitated with anti-OSTC, and the precipitates were analyzed by western blotting with anti-ATG4. IgG immunoprecipitation was used as negative control.

(B) The samples were co-precipitated with anti-CALR, and the precipitates were analyzed by western blotting with anti-ATG4.

(C) The samples were co-immunoprecipitated with anti-ATG4, and the precipitates were analyzed by western blotting with anti-LC3.

(D) The western blotting with anti-LC3. β-actin was used as the internal reference gene.

(E) The samples were co-precipitated with anti-LC3, and the precipitates were analyzed by western blotting with anti-ATG3 and anti-ATG7.

(F) The samples were co-immunoprecipitated with anti-ATG5, and the precipitates were analyzed by western blotting with anti-LC3, anti-ATG12, anti-ATG16l1, and anti-ATG9.

(G) Western blotting with anti-beclin1. β-actin was used as the internal reference gene.

(H) Autophagy LC3 HiBiT-reporter assay. The values of each group were expressed as mean ± SD (n = 3); * *p < 0.01, *p < 0.05.

(I) (a) Adenovirus Red-cherry-GFP-LC3 was infected, and autophagy was monitored. Autophagy was observed by fluorescence microscope (red marker cherry-LC3). (b) The incidence rate of autophagy was compared. Each experiment was repeated three times. The values of each group were expressed as mean ± SEM (n = 3); * *p < 0.01, *p < 0.05.J&K. Western blotting analysis was performed using anti-PAK2, anti-PLK1, anti-PRKAR2A, anti-MYBL1, anti-Trim44, anti-Sash1, and anti-Smad5. β-actin was used as the internal reference gene.

compared with rLV group, respectively (Figure S8B). Collectively, these results suggest that both CALR knockdown and excessive OSTC abrogate the carcinogenic function of miR-1307 in liver cancer cells.

DISCUSSION

In this study, our studies confirm that miR-1307 has an effect on the malignant proliferation of human hepatoma cells and indicate the effect of miR-1307 on the signal pathway network of human liver cancer cells from the perspective of epigenetic regulation omics, transcriptomics, and proteomics (Figure 9I). Furthermore, this study reveals the mechanism of miR-1307 on the proliferation of liver cancer cells by affecting the folding function of endoplasmic reticulum protein and provides new ideas for the treatment of a variety of cancers.

miR-1307 promotes human hepatocarcinogenesis

In this study, miR-1307 can significantly promote the growth of hepatoma cells *in vitro* and *in vivo*, including cell proliferation, colony forming ability, and tumorigenesis in nude mice. Tang et al. showed that miR-1307

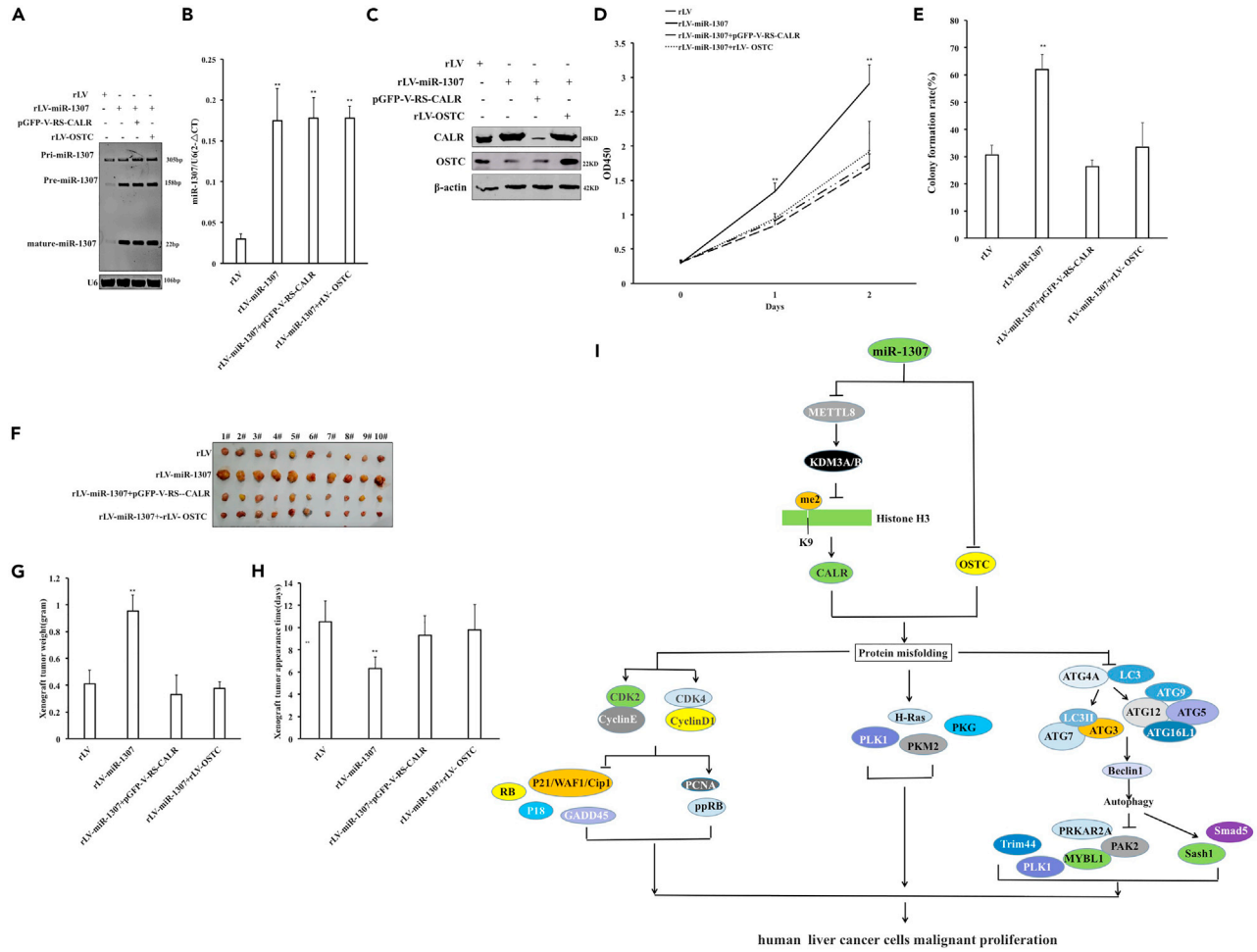

Figure 9. Both CALR knockdown and excessive OSTC abrogate the carcinogenic function of miR-1307 in liver cancer

(A) The precursor and mature miR-1307 were detected by northern blot. U6 was used as the internal reference gene.

(B) The mature miR-1307 was detected by RT-PCR. U6 was used as the internal reference gene.

(C) The CALR and OSTC were detected by western blotting. β-actin is used as internal reference.

(D) The proliferation ability was determined by CCK8. * *p < 0.01 and *p < 0.05.

(E) The colony formation ability of the cells was measured.

(F) The picture of xenograft tumor.

(G) Comparison of the size of xenograft tumors in nude mice.

(H) The appearance time (days) of xenograft tumors in nude mice was compared. The mean ± SEM (n = 10); * *p < 0.01 and *p < 0.05.

(I) Molecular mechanism of miR-1307 promoting the development of liver cancer.

promotes the occurrence of colorectal cancer by interfering with dicer recruitment (Tang et al., 2015). Studies have confirmed that miR-1307 is upregulated in colorectal cancer, breast cancer, and hepatocellular carcinoma and plays a role in promoting tumor development by regulating its downstream targets TUSC5, Smyd4, and DAB2IP in different cancers (Yue et al., 2020). Yang et al. found that miR-1307 promoted the proliferation and migration of colorectal cancer cells by inhibiting PRRX1 (Yang et al., 2020). Du et al. demonstrated that miR-1307-5p targeted TRAF3 and activated NF-κB/MAPK pathway to promote the proliferation of lung adenocarcinoma (Du et al., 2020). Qi et al. demonstrated that miR-1307 could promote the proliferation of prostate cancer by targeting FOXO3a (Qiu and Dou, 2017). Our results are consistent with the reports and further suggest that miR-1307 can promote the malignant progression of human liver cancer.

miR-1307 affects histone methylation in human liver cancer cells

In this study, anti-H3K9me2-chromatin immunoprecipitation sequencing analysis reveal the effect of miR-1307 on the epigenetic regulation in human liver cancer cells. miR-1307 changed the methylation of H3K9

on some genes, such as Wnt16, KDM1A, RAX, CDC27, CALCR, CREBBP, CDK14, TRPM3, KDM4C, Tbx22, Ube3c, Rad50, HDAC2, PRPC3C, CALN1, SOX5, TUT4, etc. These genes play an important role in tumorigenesis and development. Recent studies have shown that CDK14 is highly expressed in osteosarcoma, breast cancer, liver cancer, and other cancers (Li et al., 2019a, 2019b, 2019c). Ube3c can promote the growth and metastasis of cancer and plays an important role in cancer progression (Tao et al., 2017). SOX5 is related to the progress of liver cancer, prostate cancer, lung cancer, and other cancers (Li et al., 2019a, 2019b, 2019c). Our results suggest that miR-1307 may affect the epigenetics to regulate the expression of genes related to hepatocarcinogenesis.

miR-1307 affects transcriptomics of human liver cancer cells

RNA sequencing analysis showed that miR-1307 had a certain effect on the transcriptomics of human hepatoma cells. It was found that miR-1307 overexpression led to upregulation of some genes, such as CALR, LMNA, ATAD2, TUBA1C, CCT3, CAPZB, MCM5, CKSB1, CCNA2, ELAVL2, MARCKS, TUBB, ATP8B2, PPIG, CALR, SF3B3, PSIP1, GMPS, SCAF1, MCM4, TOP2A, PRCC, etc. Studies have confirmed that CALR is upregulated in breast cancer cells, non-small-cell lung cancer, and other cancer cells. The expression of calreticulin in stromal area of malignant tissues was significantly higher than that of the former (Zamanian et al., 2016). CCNA2 is involved in the proliferation, invasion, and differentiation of tumor cells (Li et al., 2019a, 2019b, 2019c). Some downregulated genes were found, such as OSTC, ARF5, RPS5, UBE2M, THRA, HBP1, EFNB2, KDM3A, OTUB1, ASC22D1, RPLP1, FBL, ACP1, NTN1, KCNAB2, MBTPS1, SDHA, SERPINH1, SLC6A9, MAN1A1, PRLHR, PPP2R5C, etc. KDM3A can promote the migration and invasion of tumor cells in breast cancer, cervical cancer, Ewing sarcoma, and neuroblastoma (Dandawate et al., 2019). Netrin 1 plays a key role in the migration, differentiation, and apoptosis of nerve cells. Studies have shown that the plasma concentration of Netrin 1 increases in patients with breast cancer, renal cancer, liver cancer, and other cancers (Li et al., 2020a, 2020b, 2020c, 2020d).

miR-1307 affects proteomics of human liver cancer cells

In this study, label-free quantitative proteolytic peptide mass spectrometry analysis revealed that miR-1307 changed the proteomics of human hepatoma cells. Among them, 208 genes were upregulated, and 227 genes were downregulated. The upregulated proteins include TOP2A, LPR1, RAB7A, CALU, SP1, CAVIN1, DLD, Rad21, CTCF, JUN, HSPG2, HIST1H2A, CBX, PRKAR, PPP1R7, CAVIN3, CARMIL, FOXP4, PRKAR, TBK1, FAM20B, DNMT3A, CDK2AP1, etc. It is found that RAB7ARab GTPases is a key regulator of membrane transport in the endomembrane system, and Rab7 is a key regulator of endosome biogenesis and maturation (Wang et al., 2019). Upregulation of calumenin (CALU) is associated with increased cell migration and metastasis in lung cancer and colon cancer (Nasri Nasrabadi et al., 2020).The downregulated proteins include TUBA1C, TUBB4A, PHB, XPO1, EIF5A, EIF3D, KAT7, PFKL, OGT, MTOR, PFKM, DTBP3, EIF2A, CDC16, TFAD4, CARM1, UBE4B, CCDCB4, BIN1, EIF3H, SETDB1, PPKCD, UBASH3B, etc. CARM1 is a protein arginine methyltransferase, which enhances the transcriptional activation of nuclear receptors by interacting with p160 and cAMP response element binding protein (CBP) (Porta et al., 2019). KAT7 lysine acetyltransferase 7, also known as HBO1 and MYST2, is a member of the MYST family and tends to acetylate histones at H4K5, H4K12, and H3K14 (Jie et al., 2020).

In addition, GO enrichment analysis of differential proteins was mostly involved in DNA-directed RNA polymerase II, transferase complex, protein methylation, snRNA processing, cell migration, and Ras GTPase binding and activity. KEGG signaling pathway enrichment of different proteins was mostly involved in mucin type O-glycan biosynthesis, cell cycle, calcium signaling pathway, Ras signaling pathway, PI3K signaling pathway, and autophagy. Studies have shown that autophagy plays a dynamic role in tumor inhibition or promotion in different environments and stages of cancer development (Li et al., 2020a, 2020b, 2020c, 2020d). Overexpression of miR-1307 affects the expression levels of many proteins that play an important role in tumor development, which may be the reason that miR-1307 affects the malignant proliferation of hepatoma cells.

miR-1307 affects the interaction of molecular network of CALR

In this study, the effect of miR-1307 on the interaction molecular network of endoplasmic reticulum regulatory factor CALR was revealed by using anti-CALR immunoprecipitation protein-mass spectrometry. The results showed 168 upregulated and 100 downregulated CALR binding proteins. The important ones include MYH10, TPM3, ENO3, ACLY, DDB1, CALD1, SEC233A, AP2S1, TXN, DDOST, AARS, ETF1, SDTBN1, etc. Studies have shown that TPM3 encodes a member of actin-binding protein tropomyosin

family, which provides stability for actin, and its gene mutation may lead to its oncogene function (Janco et al., 2019). DDOST gene encodes the component of oligosaccharide transferase complex, which catalyzes the transfer of high mannose oligosaccharides to asparagine residues on new peptides in rough endoplasmic reticulum (Harada et al., 2019).

In addition, GO enrichment analysis showed that the CALR binding proteins were mainly involved in calmodulin binding, oligosaccharyl transfer complex, peptidyl amino acid domain, and DNA binding. KEGG pathway enrichment analysis showed that the CALR binding proteins were mainly involved in nucleoside exercise, arginine and proline metabolism, ATP-dependent RNA helicase, dipeptidyl peptidase3, and erbB signaling pathway. Calmodulin binding protein is called calmodulin binding protein, which is involved in many cellular processes, including development of cancer (Sharma and Parameswaran, 2018). It is suggested that miR-1307 affects the interaction protein network of CALR in human hepatoma cells, which may promote the occurrence and development of live cancer.

The function of miR-1307 is related to CALR and OSTC

CALR is a pleiotropic and highly conserved molecule and is recognized as UPR effector protein. OSTC is a noncatalytic subunit of oligosaccharide transferase complex, also known as DC2. In this study, we found that the mature sequence of miR-1307 could bind to the 3′-noncoding region (2225-2232) of methyltransferase protein 8 (METTL8) mRNA through eight-base seed sequences, targeting METTL8 3′-UTR and inhibiting the translation ability of METTL8 (a member of methyltransferase-like protein family). miR-1307 inhibited the expression of KDM3A and KDM3b by reducing METTL8. KDM3A can promote the migration and invasion of breast cancer, cervical cancer, and neuroblastoma (An et al., 2019).

Moreover, miR-1307 reduced the methylation of histone H3K9 by inhibiting the expression of KDM3A and KDM3B. miR-1307 promotes the binding ability of P300 and RNA pol II to the promoter region of endoplasmic reticulum regulatory protein CALR by H3K9me2, which further promotes the transcription and translation of CALR. In addition, this study shows that miR-1307 can inhibit the expression of OSTC in hepatoma cells. In particular, rescued test confirmed that the endoplasmic-reticulum-pathway-related genes, CALR and OSTC, play an important role in the carcinogenic function of miR-1307. Therefore, it is speculated that miR-1307 may change the function of endoplasmic reticulum, induce protein misfolding, and change gene expression and function dependent on CALR and OSTC.

miR-1307 affects cellular cyclins dependent on CALR-OSTC-endoplasmic reticulum protein folding pathway

The imbalance of cell-cycle process will lead to uncontrolled cell proliferation and eventually to tumor occurrence. CDK4/6 and CyclinD1 (CCND1) form a complex of phosphorylated retinoblastoma protein (RB) and separate it from E2F transcription factor, thus promoting cell cycle. If the process is out of control, cancer will be caused (Alvarez-Fernandez and Malumbres, 2020). CCND1, as a cancer gene, can promote the proliferation of cancer cells (Zhang, 2020; Tadesse et al., 2020).

In this study, miR-1307 weakened the binding ability of OSTC with CDK2, CDK4, CyclinD1, and cyclinE and enhanced the binding ability of CALR with CDK2, CDK4, CyclinD1, and cyclinE, thus enhancing the interaction between CDK2 and cyclinE and CyclinD1 in liver cancer cells, which resulted in a significant decrease of p21waf1/cip1, GADD45, pRB, and P18 expression and a significant increase of ppRB and PCNA. P21WAF1/CIP1 is a major member of p53-dependent cell-cycle arrest induced by DNA damage (Zohny et al., 2019). However, Hep3B is a p53-null cell line, and P21WAF1/CIP1 was upregulated in Hep3B independent on P53. The combination treatment of p53-null HL-60 cells with DNA-damaging agent CLB and HDACIs NaBu and TSA triggered upregulated p21(WAF1/CIP1) expression (Kwa et al., 2019). p21(WAF1/CIP1) expression predicts outcome in p53-null ovarian carcinoma (Rose et al., 2003). p53-independent p21(WAF1/CIP1) expression causes genomic instability by deregulating replication licensing (Galanos et al., 2016). P21(CIP1/WAF1) blocks paclitaxel-induced G2M arrest and attenuates mitochondrial injury and apoptosis in p53-null human leukemia cells (Ahmed et al., 2004). Furthermore, knockout GADD45α can significantly eliminate G2/M cell-cycle stagnation and cell death induced by endoplasmic reticulum stress (Li et al., 2020a, 2020b, 2020c, 2020d). GADD45α plays a protective role in the development of tumor (Pietrasik et al., 2020). The deletion of RB gene and the deletion of expression of pRB are often observed in cancer such as esophageal squamous cell carcinoma (Wang et al., 2012). P18 has the function of tumor suppressor and also shows the inhibitory activity of PD-1/PD-L1 (Tang et al., 2020). PCNA has been reported to be highly expressed in many cancers, such as non-small-cell lung

cancer, breast cancer, etc. (Ye et al., 2020). It is suggested that miR-1307 changes the expression of cyclin-related proteins pRB, PCNA, p21waf1/cip1, GADD45, P18, and ppRB dependent on CALR-OSTC-endoplasmic reticulum protein folding pathway.

miR-1307 affects the activity of oncoproteins and protein kinases through endoplasmic reticulum protein folding pathway

In this study, we found that miR-1307 reduced the binding ability of OSTC with H-ras, PKM2, and PLK1; enhanced the binding ability of CALR with H-ras, PKM2, and PLK1; and increased the expression ability of H-ras, PKM2, and PLK1 and their activities in hepatoma cells. However, it was found that the above effects of miR-1307 were abolished after the addition of protein misfolding inhibitor. Carcinogenic Ras mutations have three isotypes: HRAS, KRAS, and NRAS, which are the background of many tumorigenesis (Kumazaki et al., 2020). PKM2 is highly expressed in a variety of human tumor cells, which provides favorable conditions for the survival, growth, and diffusion of tumor cells (Nandi and Dey, 2020). PLK1 is overexpressed in a variety of human cancers, which can directly participate in the cell-cycle regulation of tumor cells (Goroshchuk et al., 2020). These results suggest that miR-1307 affects the activities of oncoproteins and protein kinases (H-ras, PKM2 and PLK1) via the CALR-OSTC-endoplasmic reticulum protein folding pathway, thus promoting the progress of HCC.

miR-1307 inhibits autophagy via endoplasmic reticulum protein folding pathway, which affects oncogenes and tumor suppressor genes

Our results show that miR-1307 affects autophagy by CALR-OSTC-endoplasmic reticulum protein folding pathway. First, miR-1307 reduced the binding ability of OSTC with ATG4 and enhanced the binding ability of CALR with ATG4. However, protein misfolding inhibitors abolished these effects. Most studies have shown that ATG4B is more efficient in regulating autophagy through ATG8 substrate (Yang et al., 2021). ATG4B may play an important role in the occurrence and development of cancer (Fu et al., 2019).

The experimental results showed that miR-1307 reduced the binding ability of ATG4 with LC3 and the activation ability of LC3 in hepatoma cells, thus weakening the binding ability of LC3 to ATG3 and ATG7 and further inhibiting the interaction among ATG5, ATG16L1, ATG12, ATG9, and ATG7. Moreover, the protein misfolding inhibitor eliminated the above effects. LC3 is a soluble microtubule-associated protein, which can be used as a positive reference for autophagy (Yang et al., 2015). Studies have shown that LC3 expression in hepatocellular carcinoma is significantly upregulated (Ye et al., 2021). ATG5 encodes a protein that binds to autophagy protein 12 and regulates the differentiation of mesenchymal stem cells (Li et al., 2020a, 2020b, 2020c, 2020d). ATG16L1 is a part of the protein complex required for autophagy, and its gene polymorphism is related to the occurrence of a variety of cancers, such as thyroid cancer and gastric cancer (Reuken et al., 2019). ATG12 can promote autophagy by forming covalent complexes with other autophagy mediators such as ATG5 (Yoo et al., 2018). Studies have shown that ATG9 regulates the polymerization of ENA and profilins (Kiss et al., 2020). miR-1307 inhibits autophagy by affecting autophagy-related proteins through the CALR-OSTC-endoplasmic reticulum protein folding pathway.

In addition, the autophagy inhibitor miR-1307 increased the expression of PAK2, PLK1, PRKAR2A, MYBL1, and Trim44 and inhibited the expression of Sash1 and Smad5. It has been reported that miR-4779 inhibits the growth of cancer cells by targeting PAK2 and CCND3 (Koo and Kwon, 2018). Mybl1 and Myb gene rearrangement is a biomarker of tracheobronchial adenoid cystic carcinoma (Pei et al., 2019). PRKAR2A is a camp-dependent type II regulatory subunit of protein kinase, and studies have shown that its expression is related to colorectal cancer, adipocyte differentiation, and other processes (Spracklen et al., 2019). It was found that the mRNA expression level of Trim44 in most malignant tumor tissues was higher than that in corresponding normal tissues (Xiao et al., 2020). Sash1 is an adaptor and signal transduction protein, which is considered as a tumor suppressor (Ilnitskaya et al., 2020). Smad5 is involved in the proliferation of cancer cells and the internalization of extracellular matrix in tumor microenvironment (He et al., 2020; Xu et al., 2020; Zhu et al., 2020). These results suggest that miR-1307 inhibits autophagy through endoplasmic reticulum protein folding pathway, promotes the expression of oncogenes (PAK2, PLK1, PRKAR2A, MYBL1, Trim44), suppresses the expression of tumor suppressor genes (Sash1, Smad5) in hepatoma cells, and ultimately promotes the malignant proliferation of hepatoma cells.

In summary, this study confirmed that miR-1307 could significantly enhance the malignant proliferation ability of human hepatoma cells and revealed that miR-1307 could alter the expression of some genes,

especially some endoplasmic-reticulum-pathway-related genes such as CALR and OSTC. These results provide a theoretical basis for further study of the detailed molecular mechanism of miR-1307 promoting the occurrence and development of liver cancer.

Limitations of the study

In the study presented here, we provide comprehensive evidences that miR-1307 can significantly enhance the malignant proliferation ability of human liver cancer cells and revealed that miR-1307 could alter the expression of some genes, especially some endoplasmic-reticulum-pathway-related genes such as CALR and OSTC. However, we will further explore this mechanism and provide novel ideas for the research of liver cancer.

STAR★METHODS

Detailed methods are provided in the online version of this paper and include the following:

- KEY RESOURCES TABLE
- RESOURCE AVAILABILITY
  - Lead contact
  - Materials availability
  - Data and code availability
- EXPERIMENTAL MODEL AND SUBJECT DETAILS
- METHODS DETAILS
  - Expression Lentivirus for human miR-1307
  - RT-PCR
  - RNA immunoprecipitation (RIP)
  - Super-RNA-EMSA
  - CHIP assay
  - Autophagy LC3 inhibit reporter assay
  - Autophagy detection by adenovirus infection
  - Cell colony-formation efficiency assay
  - Tumorigenesis test *in vivo*
  - Chip-Seq
  - RNA sequencing analysis
  - Mass spectrometric analysis
  - Immunoprecipitation protein mass spectrometry
  - RIP-sequencing analysis
- QUANTIFICATION AND STATISTICAL ANALYSIS
  - Statistical analysis

SUPPLEMENTAL INFORMATION

Supplemental information can be found online at https://doi.org/10.1016/j.isci.2021.103271.

ACKNOWLEDGMENTS

This study was supported by grants from National Natural Science Foundation of China (NCSF No.81773158, NCSF No.82073130), Science and Technology Commission of Shanghai Municipality Shanghai Science and Technology Plan Basic Research Field Project (19JC1415200), and Science and Technology Commission of Shanghai Municipality Shanghai Science and Technology Plan Basic Research Field Project (20JC1411400).

AUTHOR CONTRIBUTIONS

Conceptualization, D.D.L.; Methodology, D.D.L.; Investigation, S.J.X., X.X.J., R.S.Q., S.T.S., Y.N.L., L.Y.W., Y.J.C.; Writing—Original Draft, D.D.L.; Writing—Review & Editing, D.D.L.; Funding acquisition, D.D.L. All authors have read and approved the final manuscripts.

DECLARATION OF INTERESTS

The authors declare no competing interests.

Received: May 17, 2021
Revised: August 27, 2021
Accepted: October 12, 2021
Published: November 19, 2021

REFERENCES

Ahmed, W., Rahmani, M., Dent, P., and Grant, S. (2004). The cyclin-dependent kinase inhibitor p21(CIP1/WAF1) blocks paclitaxel-induced G2M arrest and attenuates mitochondrial injury and apoptosis in p53-nullhuman leukemia cells. Cell Cycle *3*, 1305–1311.

Alvarez-Fernandez, M., and Malumbres, M. (2020). Mechanisms of sensitivity and resistance to CDK4/6 inhibition. Cancer Cell *37*, 514–529.

An, M.J., Kim, D.H., and Kim, C.H. (2019). Histone demethylase KDM3B regulates the transcriptional network of cell-cycle genes in hepatocarcinoma HepG2 cells. Biochem. Biophys. Res. Commun. *508*, 576–582.

Balmeh, N., Mahmoudi, S., and Mohammadi, N. (2020). Predicted therapeutic targets for COVID-19 disease by inhibiting SARS-CoV-2 and its related receptors. Inform Med. Unlocked *20*, 100407.

Dandawate, P., Ghosh, C., and Palaniyandi, K. (2019). The histone demethylase KDM3A, increased in human pancreatic tumors, regulates expression of DCLK1 and promotes tumorigenesis in mice. Gastroenterology *157*, 1646–1659.e11.

Deng, W., Fu, J., and Wang, T. (2020). Hsa_circRNA_101036 acts as tumor-suppressor in oral squamous cell carcinoma cells via inducing endoplasmic reticulum stress. Eur. Rev. Med. Pharmacol. Sci. *24*, 6111–6121.

Du, X., Wang, S., and Liu, X. (2020). MiR-1307-5p targeting TRAF3 upregulates the MAPK/NF-kappaB pathway and promotes lung adenocarcinoma proliferation. Cancer Cell Int. *20*, 502.

Fu, Y., Hong, L., and Xu, J. (2019). Discovery of a small molecule targeting autophagy via ATG4B inhibition and cell death of colorectal cancer cells in vitro and in vivo. Autophagy *15*, 295–311.

Galanos, P., Vougas, K., Walter, D., Polyzos, A., Maya-Mendoza, A., Haagensen, E.J., Kokkalis, A., Roumelioti, F.M., Gagos, S., Tzetis, M., et al. (2016). Chronic p53-independent p21 expression causes genomic instability by deregulating replication licensing. Nat. Cell Biol *18*, 777–789.

Goroshchuk, O., Vidarsdottir, L., and Bjorklund, A.C. (2020). Targeting Plk1 with siRNNs in primary cells from pediatric B-cell acute lymphoblastic leukemia patients. Sci. Rep. *10*, 2688.

Harada, Y., Ohkawa, Y., and Kizuka, Y. (2019). Oligosaccharyltransferase: a gatekeeper of health and tumor progression. Int. J. Mol. Sci. *20*, 6074.

He, W., Li, F., and Zhang, S. (2020). LncRNA AFAP1-AS1 promotes osteoblast differentiation of human aortic valve interstitial cells through regulating miR-155/SMAD5 axis. Mol. Cell Probes *50*, 101509.

Ilnitskaya, A.S., Zhitnyak, I.Y., and Gloushankova, N.A. (2020). Involvement of SASH1 in the maintenance of stable cell-cell adhesion. Biochemistry (Mosc) *85*, 660–667.

Janco, M., Rynkiewicz, M.J., and Li, L. (2019). Molecular integration of the anti-tropomyosin compound ATM-3507 into the coiled coil overlap region of the cancer-associated Tpm3.1. Sci. Rep. *9*, 11262.

Jie, M., Wu, Y., and Gao, M. (2020). CircMRPS35 suppresses gastric cancer progression via recruiting KAT7 to govern histone modification. Mol. Cancer *19*, 56.

Kiss, V., Jipa, A., and Varga, K. (2020). Drosophila Atg9 regulates the actin cytoskeleton via interactions with profilin and Ena. Cell Death Differ. *27*, 1677–1692.

Koo, K.H., and Kwon, H. (2018). MicroRNA miR-4779 suppresses tumor growth by inducing apoptosis and cell cycle arrest through direct targeting of PAK2 and CCND3. Cell Death Dis. *9*, 77.

Kumazaki, M., Shimomura, I., and Kiyono, T. (2020). Cell-type specific tumorigenesis with Ras oncogenes in human lung epithelial cells. Biochem. Biophys. Res. Commun. *525*, 483–490.

Kwa, F.A.A., Cole-Sinclair, M.F., and Kapuscinski, M.K. (2019). Combination treatment of p53-null HL-60 cells with histone deacetylase inhibitors and augments apoptosis and increases BCL6 and p21Gene expression. Curr. Mol. Pharmacol. *12*, 72–81.

Li, G., Wang, K., and Wang, J. (2019a). miR-497-5p inhibits tumor cell growth and invasion by targeting SOX5 in non-small-cell lung cancer. J. Cell Biochem. *120*, 10587–10595.

Li, J., Shao, W., and Feng, H. (2019b). MiR-542-3p, a microRNA targeting CDK14, suppresses cell proliferation, invasiveness, and tumorigenesis of epithelial ovarian cancer. Biomed. Pharmacother. *110*, 850–856.

Li, X., Ma, X.L., and Tian, F.J. (2019c). Downregulation of CCNA2 disturbs trophoblast migration, proliferation, and apoptosis during the pathogenesis of recurrent miscarriage. Am. J. Reprod. Immunol. *82*, e13144.

Li, B., Shen, K., and Zhang, J. (2020a). Serum netrin-1 as a biomarker for colorectal cancer detection. Cancer Biomark *28*, 391–396.

Li, J., Li, Y., and Zhan, X.Y. (2020b). Generation of GADD45A gene knockout human embryonic stem cell line using CRISPR/Cas9. Stem Cell Res. *49*, 102090.

Li, X., He, S., and Ma, B. (2020c). Autophagy and autophagy-related proteins in cancer. Mol. Cancer *19*, 12.

Li, Y., Jiang, Y., and Cheng, J. (2020d). ATG5 regulates mesenchymal stem cells differentiation and mediates chemosensitivity in acute myeloid leukemia. Biochem. Biophys. Res. Commun. *525*, 398–405.

Liu, J., Fan, L., and Yu, H. (2019). Endoplasmic reticulum stress causes liver cancer cells to release exosomal miR-23a-3p and up-regulate programmed death ligand 1 expression in macrophages. Hepatology *70*, 241–258.

Moenner, M., Pluquet, O., and Bouchecareilh, M. (2007). Integrated endoplasmic reticulum stress responses in cancer. Cancer Res. *67*, 10631–10634.

Nandi, S., and Dey, M. (2020). Biochemical and structural insights into how amino acids regulate pyruvate kinase muscle isoform 2. J. Biol. Chem. *295*, 5390–5403.

Nasri Nasrabadi, P., Nayeri, Z., and Gharib, E. (2020). Establishment of a CALU, AURKA, and MCM2 gene panel for discrimination of metastasis from primary colon and lung cancers. PLoS One *15*, e0233717.

Oakes, S.A. (2017). Endoplasmic reticulum proteostasis: a key checkpoint in cancer. Am. J. Physiol. Cell Physiol *312*, C93–C102.

Oakes, S.A. (2020). Endoplasmic reticulum stress signaling in cancer cells. Am. J. Pathol. *190*, 934–946.

Oakes, S.A., and Papa, F.R. (2015). The role of endoplasmic reticulum stress in human pathology. Annu. Rev. Pathol. *10*, 173–194.

Pei, J., Flieder, D.B., and Patchefsky, A. (2019). Detecting MYB and MYBL1 fusion genes in tracheobronchial adenoid cystic carcinoma by targeted RNA-sequencing. Mod. Pathol. *10*, 1416–1420.

Pietrasik, S., Zajac, G., and Morawiec, J. (2020). Interplay between BRCA1 and GADD45A and its potential for nucleotide excision repair in breast cancer pathogenesis. Int. J. Mol. Sci. *21*, 870.

Porta, M., Amione, C., and Barutta, F. (2019). The co-activator-associated arginine methyltransferase 1 (CARM1) gene is overexpressed in type 2 diabetes. Endocrine *63*, 284–292.

Qiu, X., and Dou, Y. (2017). miR-1307 promotes the proliferation of prostate cancer by targeting FOXO3A. Biomed. Pharmacother. *88*, 430–435.

Reuken, P.A., Lutz, P., and Casper, M. (2019). The ATG16L1 gene variant rs2241880 (p.T300A) is associated with susceptibility to HCC in patients with cirrhosis. Liver Int. *39*, 2360–2367.

Rose, S.L., Goodheart, M.J., DeYoung, B.R., Smith, B.J., and Buller, R.E. (2003). p21 expression

predicts outcome in p53-null ovarian carcinoma. Clin. Cancer Res. *9*, 1028–1032.

Ruan, D.T., Gao, S., and Shelat, H. (2020). Differential expression of microRNA and arachidonic acid metabolism in aspirin-treated human cardiac and peri-cardiac fat-derived mesenchymal stem cells. Vascul Pharmacol. *127*, 106651.

Sharma, R.K., and Parameswaran, S. (2018). Calmodulin-binding proteins: a journey of 40 years. Cell Calcium *75*, 89–100.

Spracklen, C.N., Karaderi, T., and Yaghootkar, H. (2019). Exome-derived adiponectin-associated variants implicate obesity and lipid biology. Am. J. Hum. Genet. *105*, 15–28.

Su, Y.Y., Sun, L., and Guo, Z.R. (2019). Upregulated expression of serum exosomal miR-375 and miR-1307 enhance the diagnostic power of CA125 for ovarian cancer. J. Ovarian Res. *12*, 6.

Tadesse, S., Anshabo, A.T., and Portman, N. (2020). Targeting CDK2 in cancer: challenges and opportunities for therapy. Drug Discov. Today *25*, 406–413.

Takamura, Y., Aoki, W., and Satomura, A. (2018). Small RNAs detected in exosomes derived from the MH7A synovial fibroblast cell line with TNF-alpha stimulation. PLoS ONE *13*, e0201851.

Tang, J., Meng, Q., and Shi, R. (2020). PRMT6 serves an oncogenic role in lung adenocarcinoma via regulating p18. Mol. Med. Rep. *22*, 3161–3172.

Tang, R., Qi, Q., and Wu, R. (2015). The polymorphic terminal-loop of pre-miR-1307 binding with MBNL1 contributes to colorectal carcinogenesis via interference with Dicer1 recruitment. Carcinogenesis *36*, 867–875.

Tao, J., Liu, Z., and Wang, Y. (2017). MiR-542-3p inhibits metastasis and epithelial-mesenchymal transition of hepatocellular carcinoma by targeting UBE3C. Biomed. Pharmacother. *93*, 420–428.

Wang, G., Hu, H.B., and Chang, Y. (2019). Rab7 regulates primary cilia disassembly through cilia excision. J. Cell Biol. *218*, 4030–4041.

Wang, M., and Kaufman, R.J. (2016). Protein misfolding in the endoplasmic reticulum as a conduit to human disease. Nature *529*, 326–335.

Wang, M.T., Chen, G., and An, S.J. (2012). Prognostic significance of cyclinD1 amplification and the co-alteration of cyclinD1/pRb/ppRb in patients with esophageal squamous cell carcinoma. Dis. Esophagus *25*, 664–670.

Xiao, G., Yang, Q., and Bao, Z. (2020). Expression of tripartite motif-containing 44 and its prognostic and clinicopathological value in human malignancies:a meta-analysis. BMC cancer *20*, 525.

Xu, T., Luo, Y., and Wang, J. (2020). Exosomal miRNA-128-3p from mesenchymal stem cells of aged rats regulates osteogenesis and bone fracture healing by targeting Smad5. J. Nanobiotechnology *18*, 47.

Yang, G., Li, Y., and Zhao, Y. (2021). Targeting Atg4B for cancer therapy: chemical mediators. Eur. J. Med. Chem. *209*, 112917.

Yang, M., Liu, X., and Meng, F. (2020). The rs7911488-T allele promotes the growth and metastasis of colorectal cancer through modulating miR-1307/PRRX1. Cell Death Dis. *11*, 651.

Yang, Z., Li, R., and Ao, J. (2018). miR-1307-3p suppresses the chondrogenic differentiation of human adipose-derived stem cells by targeting BMPR2. Int. J. Mol. Med. *42*, 3115–3124.

Yang, Z., Wilkie-Grantham, R.P., and Yanagi, T. (2015). ATG4B (Autophagin-1) phosphorylation modulates autophagy. J. Biol. Chem. *290*, 26549–26561.

Ye, X., Ling, B., and Xu, H. (2020). Clinical significance of high expression of proliferating cell nuclear antigen in non-small cell lung cancer. Medicine (Baltimore) *99*, e19755.

Ye, Y., Tyndall, E.R., and Bui, V. (2021). An N-terminal conserved region in human Atg3 couples membrane curvature sensitivity to conjugase activity during autophagy. Nat. Commun. *12*, 374.

Yoo, B.H., Khan, I.A., and Koomson, A. (2018). Oncogenic RAS-induced downregulation of ATG12 is required for survival of malignant intestinal epithelial cells. Autophagy *14*, 134–151.

Yue, N., Ye, M., and Zhang, R. (2020). MicroRNA-1307-3p accelerates the progression of colorectal cancer via regulation of TUSC5. Exp. Ther. Med. *20*, 1746–1751.

Zamanian, M., Qader Hamadneh, L.A., and Veerakumarasivam, A. (2016). Calreticulin mediates an invasive breast cancer phenotype through the transcriptional dysregulation of p53 and MAPK pathways. Cancer Cell Int *16*, 56.

Zhang, H. (2020). CCND1 silencing suppresses liver cancer stem cell differentiation through inhibiting autophagy. Hum. Cell *33*, 140–147.

Zhao, T., Du, J., and Zeng, H. (2020). Interplay between endoplasmic reticulum stress and non-coding RNAs in cancer. J. Hematol. Oncol. *13*, 163.

Zheng, Y., Zheng, Y., and Lei, W. (2019). miR-1307-3p overexpression inhibits cell proliferation and promotes cell apoptosis by targeting ISM1 in colon cancer. Mol. Cell Probes *48*, 101445.

Zhou, Y., Wang, M., and Shuang, T. (2019). MiR-1307 influences the chemotherapeutic sensitivity in ovarian cancer cells through the regulation of the CIC transcriptional repressor. Pathol. Res. Pract. *215*, 152606.

Zhou, Y., Wang, M., Wu, J., Jie, Z., Chang, S., and Shuang, T. (2015). The clinicopathological significance of miR-1307 in chemotherapy resistant epithelial ovarian cancer. J. Ovarian Res. *8*, 23.

Zhu, Z., Achreja, A., and Meurs, N. (2020). Tumour-reprogrammed stromal BCAT1 fuels branched-chain ketoacid dependency in stromal-rich PDAC tumours. Nat. Metab. *2*, 775–792.

Zohny, S.F., Al-Malki, A.L., and Zamzami, M.A. (2019). p21(Waf1/Cip1): its paradoxical effect in the regulation of breast cancer. Breast Cancer *26*, 131–137.

STAR★METHODS

KEY RESOURCES TABLE

REAGENT or RESOURCE	SOURCE	IDENTIFIER
Antibodies		
Anti-METTL8	Abcam	Cat#ab122273
Anti-KDM3A/JHDM2A	Abcam	Cat#ab191389
Anti-KDM3B/JMJD1B	Abcam	Cat#ab70797
Anti-H3K9me1	Abcam	Cat#ab176880
Anti-H3K9me2	Abcam	Cat#ab1220
Anti-H3K9me3	Abcam	Cat#ab8898
Anti-Histone H3	Abcam	Cat#ab1791
Anti-Calreticulin	Abcam	Cat#ab92516
Anti-cyclin D1 (A-12)	santa cruz	Cat#sc-450
Anti-Cdk2	Abcam	Cat#ab32147
Anti-Cyclin E1	Abcam	Cat#ab33911
Anti-Cdk4 (DCS-35)	santa cruz	Cat#sc-23896
Anti-p21 Waf1/Cip1	santa cruz	Cat#sc-187
Anti-GADD 45α	santa cruz	Cat#sc-6850
Anti-Rb (C-2)	santa cruz	Cat#sc-74562
Anti-p-Rb	santa cruz	Cat#sc-377540
Anti-PCNA	santa cruz	Cat#sc-25280
Anti- p18 (INK4c)	santa cruz	Cat#sc-9965
Anti-H-Ras	santa cruz	Cat#sc-35
Anti-PKM2	Abcam	Cat#ab85555
Anti-PLK1	Abcam	Cat#ab189139
Anti-cGKIα/β	santa cruz	Cat#sc-271766
Anti-MAP LC3α/β	santa cruz	Cat#sc-398822
Anti-ATG4A	Abcam	Cat#ab108322
Anti-ATG7	Abcam	Cat#ab52472
Anti-ATG3	Abcam	Cat#ab108251
Anti-APG5L/ATG5	Abcam	Cat#ab108327
Anti-ATG12	Abcam	Cat#ab109491
Anti-ATG9A	Abcam	Cat#ab108338
Anti-ATG16L1	Abcam	Cat#ab187671
Anti-Beclin-1/BECN1	santa cruz	Cat#sc-48341
Anti-PRK2	santa cruz	Cat#sc-271971
Anti-PKA R2/PKR2	Abcam	Cat#ab32514
Anti-v-Myb/a-Myb	santa cruz	Cat#sc-73246
Anti-SASH1	santa cruz	Cat#sc-517001
Anti-Smad5	santa cruz	Cat#SC-101151
Anti-TRIM44	Abcam	Cat#ab236422
Anti-OSTC	Invitrogen	Cat#PA5-95894
Experimental models		
Hep3B cell line	ATCC	N/A
Athymic Balb/c mice	SLAC	SYXK2009-002

(*Continued on next page*)

Continued

REAGENT or RESOURCE	SOURCE	IDENTIFIER
Recombinant DNA		
rLV-miR1307	Venuosai	N/A
Ad-cherry-GFP-LC3	Beyotime	Cat#C3011
pLVX-miR-1307	Venuosai	N/A
pGFP-V-RS	Origene	Cat#TR30007
pMirTarget	Origene	Cat#PS100062
Chemicals, peptides, and recombinant proteins		
DMEM	BIOAGRIO	Cat#LD1111-500
PBS	BIOAGRIO	Cat#LS2041-500
0.25%Trypsin-EDTA	BIOAGRIO	Cat#LT1721
Fetal bovine serum	BIOAGRIO	Cat#S1001-500
CCK8	BIOAGRIO	Cat#CK192-500
Trizol	TIANGEN	Cat#DP424
Tris-HCl/SDS (PH6.8)	Sangon	Cat#SD8022
Tris-HCl/SDS (PH8.8)	Sangon	Cat#SD8021
Crystal Violet	Sangon	Cat#524-62-9
SDS-PAGE gel (10%)	Epizyme	Cat#PG112
PIPA lysate	Beyotime	Cat#P0013
Protein loading buffer	Beyotime	Cat#P001513
Lipofectamine2000	Invitrogen	Cat#P/LS2887
Cocktail inhibitor	Beyotime	Cat#B14011
Protein A/G agarose	santa cruz	Cat#sc-2003
Nitrocellulose membrane	Beyotime	Cat#FFN08
BIX-01294	MCE	Cat#935693-62-2
Flubendazole	Selleck	Cat#SJ00206711979
Critical commercial assays		
RT-PCR kit	TIANGEN	Cat#KR106-02
miR qPCR kit	TIANGEN	Cat#FP411-01
miR RT kit	TIANGEN	Cat#KR211-01
DAB kit	Beyotime	Cat#P0202
ECL kit	Share-Bio	Cat#sb-wb012
CHIP assay kit	Beyotime	Cat#2078
BCA assay kit	Beyotime	Cat#P0012
Luciferase assay kit	Beyotime	Cat#RG027
EMSA/ gel shift kit	Beyotime	Cat#GS002
Autophagy LC3 hibit reporter assay kit	Promega	Cat#GA1040
Oligonucleotides		
Pre-miR-1307 primers:	GENEWIZ	N/A
F:5′CAUCAAGACCCAGCUGAGUC-3′		
R:5′GTCACCAGAACAAGAGCTGA-3′		
Mature miR-1307 primer:	GENEWIZ	N/A
F:5′ACTCGGCGTGGCGTCGGTCGTG-3′		
METTL8 primers:	GENEWIZ	N/A
F:5′- TCCCGTGCTAAAGGTACTGC -3′		

(*Continued on next page*)

Continued

REAGENT or RESOURCE	SOURCE	IDENTIFIER
R:5′- CTCCACAGCTCCAGAAGCAA -3′		
KDM3A primers:	Sangon	N/A
F:5′- CCTCCTGAACTGCAGAAGCA -3′		
R:5′- CAACCTGTCTGTGTGGCTCA -3′		
KDM3B primers:	GENEWIZ	N/A
F:5′- TGCTGTTCGCGGACACTG -3′		
R:5′- ACCCATTGGCATCTGACAGG -3′		
CALR primers:	GENEWIZ	N/A
F:5′- ACGATGAGGCATACGCTGAG -3′		
R:5′- ATCCACCCCAAATCCGAACC -3′		

RESOURCE AVAILABILITY

Lead contact

Further information and requests for resources and reagents should be directed to and will be fulfilled by the lead contact, Dongdong Lu (ludongdong@tongji.edu.cn). Address: Tongji University School of Life Science and Technology, Shanghai (200092), China.

Materials availability

This study did not generate new unique reagents.

Data and code availability

No custom code, software, or algorithm were used in this research. This study did not generate new code. Any additional information required to reanalyze the data reported in this paper is available from the lead contact upon request.

EXPERIMENTAL MODEL AND SUBJECT DETAILS

Cell line: human liver cancer cell line Hep3B cell line (ATCC).

Athymic Balb/c mice: SLAC (SYXK2009-002).

All methods were carried out in "accordance" with the approved guidelines. All experimental protocols "were approved by" a Tongji university institutional committee. Informed consent was obtained from all subjects. The study was reviewed and approved by the China national institutional animal care and use committee.

METHODS DETAILS

Expression Lentivirus for human miR-1307

The vector plasmid pLVX-miR-ZsGreen-Puro (Wuhan Venuosai Biotechnology Co., Ltd.) and the target gene plasmid pUC57-has-miR-1307 was double-digested with SpeI and NotI, respectively, and the large fragment of plasmid pLVX-miR-ZsGreen-Puro and the small fragment of plasmid pUC57-has- miR-1307 was recovered by 1% agarose gel electrophoresis. The two plasmid fragments were performed ligation reaction at 22 ° C for 3 hours, and the ligation product was transformed into JM109 competent bacterial and cultured overnight. The recombinant plasmid pLVX-miR-1307- ZsGreen-Puro containing the gene of interest was transfected into 293 T cells, respectively, generating a lentivirus containing a gene of interest at a high titer (rLV-miR-1307).

RT-PCR

cDNA was prepared by using oligonucleotide (dT), random primers, and a SuperScript First-Strand Synthesis System. PCR analysis was performed according to the manufacturer. β-actin was used as an internal control.

Western Blotting Proteins were separated on a 10% sodium dodecyl sulfate-polyacrylamide gel electrophoresis (SDS-PAGE) and transferred onto a nitrocellulose membranes. And then blocked in 10% dry milk-TBST (20mM Tris-HCl [PH 7.6], 127mM NaCl, 0.1% Tween 20) for 1 h at 37°C. Following three washes in Tris-HCl pH 7.5 with 0.1% Tween 20, the blots were incubated with antibody (appropriate dilution) overnight at 4°C. Signals were visualized by enhanced chemiluminescence plus kit (Beyotime Biotechnology).

RNA immunoprecipitation (RIP)

Ribonucleoprotein particle-enriched lysates were incubated with protein G/A-plus agarose beads (Santa Cruz) together with antibody or normal rabbit IgG for 4 hours at 4°C. Beads were subsequently washed. RNAs were isolated and then RT-PCR.

Super-RNA-EMSA

Cells were washed and scraped in ice-cold PBS to prepare nuclei for electrophoretic gel mobility shift assay with the use of the gel shift assay system (Beyotime Biotechnology) modified according to the manufacturer's instructions.

CHIP assay

Cells were cross-linked with 1% (v/v) formaldehyde (Sigma) for 10 min at room temperature and stopped with 125 mM glycine for 5 min. Crossed-linked cells were washed with phosphate-buffered saline, resuspended in lysis buffer, and sonicated for 10 min in a SONICS VibraCell to generate DNA fragments. Chromatin extracts were diluted 6-fold with dilution buffer, pre-cleared with Protein-A/G-Sepharose beads, and immunoprecipitated with specific antibody on Protein-A/G-Sepharose beads. After washing, elution and de-cross-linking, the ChIP DNA was detected by PCR.

Autophagy LC3 inhibit reporter assay

The autophagy LC3 inhibit reporter vector (autophagy LC3 hibit reporter contains human LC3b, N-terminal hibit tag, and the intermediate "spacer" region that enhances the reporter gene specificity in autophagy pathway) was transfected into cells, and stable cell lines were screened. At the density of 20000 cells per well, the transfected autophagy LC3 inhibit reporter cells were placed on all white 96 well plates. After the cells attached overnight, the luminescence signal was measured. The stronger the luminescence signal, the lower the autophagy.

Autophagy detection by adenovirus infection

The cells were infected with rAd-cherry-GFP-LC3 and autophagy was observed 24 hours later according to the manufacturer operation manual of Beyotime Biotechnology company.

Cell colony-formation efficiency assay

cells were plated in six wells and incubated in a humidified atmosphere of 5% CO_2 incubator at 37°C for 10 days. For visualization, colonies were stained with 0.5% Crystal Violet (Sangon) in 50% methanol and 10% glacial acetic acid. Colonies were counted using a dissecting microscope by MacBiophotonics ImageJ.

Tumorigenesis test *in vivo*

Four-weeks male athymic Balb/c mice were maintained in the Tongji university animal facilities approved by the China Association for accreditation of laboratory animal care. athymic Balb/c mice per group were injected at the armpit area subcutaneously with cells. The mice were observed over 4 weeks for tumor formation. The mice were then sacrificed and the tumors recovered. The wet weight of each tumor was determined for each mouse. A portion of each tumor was fixed in 4% paraformaldehyde and embedded in paraffin for histological examination.

Chip-Seq

CHIP sequencing analysis with anti-H3K9me2 was performed according to according to the manufacturer operation manual (Novogene Co., Ltd., Beijing Nuohe Zhiyuan Technology Co., Ltd.)

RNA sequencing analysis

RNA sequencing analysis was performed according to according to the manufacturer operation manual (Novogene Co., Ltd., Beijing Nuohe Zhiyuan Technology Co., Ltd.)

Mass spectrometric analysis

Mass spectrometric analysis of enzyme hydrolyzed peptides of protein without label free was performed according to according to the manufacturer operation manual (Novogene Co., Ltd., Beijing Nuohe Zhiyuan Technology Co., Ltd.)

Immunoprecipitation protein mass spectrometry

Immunoprecipitation protein mass spectrometry analysis with anti-CALR was performed according to according to the manufacturer operation manual (Novogene Co., Ltd., Beijing Nuohe Zhiyuan Technology Co., Ltd.)

RIP-sequencing analysis

RIP-sequencing analysis with anti-METTL8 was performed according to according to the manufacturer operation manual (Novogene Co., Ltd., Beijing Nuohe Zhiyuan Technology Co., Ltd.)

QUANTIFICATION AND STATISTICAL ANALYSIS

Statistical analysis

Each value was presented as mean $\pm$ standard error of the mean (SEM) unless otherwise noted, with a minimum of three replicates. The results were evaluated by SPSS22.0 statistical soft (SPSS Inc Chicago, IL) and Student's t-test was used for comparisons, with $p < 0.05$ or $p < 0.01$ considered significant.